

FORMATION AND EVOLUTION OF THE STREAM OF SOHO KREUTZ SUNGRAZERS. II. RESULTS AND IMPLICATIONS OF MONTE CARLO SIMULATION

ZDENEK SEKANINA
La Canada Flintridge, California 91011, U.S.A.; ZdenSek@gmail.com
Version April 2, 2024

ABSTRACT

I present the results of the first comprehensive effort aimed at modeling a major component of the stream of SOHO sungrazers, 5000 of which have been detected by the onboard coronagraphs since 1996. The stream of Population I of the Kreutz system, investigated by a Monte Carlo simulation technique, is treated as a product of cascading fragmentation due to unstable rotation of a “seed,” a subkilometer-sized object that separated with others from comet X/1106 C1 at perihelion. The stream’s activity is predicted to last for 200 years from ~1950 to ~2150, culminating in the 2010s, when a swarm of bright SOHO sungrazers (peak mags not fainter than 3) of Population I was observed. By the end of 2023 about 42 percent of the stream had already arrived. Scatter amounts to 7° in the longitude of the ascending node and at most $0.2 R_\odot$ in the perihelion distance. On its initial orbit the seed would pass perihelion in 2036, 193 years after C/1843 D1, the principal fragment of X/1106 C1. Comet C/1668 E1 is proposed as another major fragment and yet another is predicted to arrive in the 2050s or 2060s.

Subject headings: individual comets: X/1106 C1, C/1668 E1, X/1702 D1, C/1843 D1, C/1882 R1, C/1887 B1, C/1963 R1, C/1965 S1, C/2011 W3; methods: data analysis

1. INTRODUCTION

To model any class of cosmic objects is risky, because models are tested by the degree of their compatibility with the results of observations, which are a function of time. A model may be consistent with existing data one day, but get in conflict with new data the next day. To model a process of formation and evolution is particularly perilous because of the delicate nature of the subject. It is recalled that the discovery and strength of the stream of Kreutz sungrazers in images taken by the LASCO coronagraphs on board the Solar and Heliospheric Observatory (SOHO) was a surprise, even though a fair number of similar (though brighter) sungrazers was detected by coronagraphs on board two previously launched spacecraft, operational over a decade only years before SOHO began its mission. Yet, it did not take long and the space observatory became the most prolific discoverer of comets. And even though SOHO has been imaging all sorts of comets, the members of the Kreutz system prevail by a wide margin.

A model for the formation and evolution of the sungrazer stream, the observed part of which contains at present approximately 4300 objects, most of them discovered over a period of 28 years, needs to be conceptually anchored. Accordingly, aiming at understanding the attributes of the stream, I provide a comprehensive description of the proposed rationale, including features of the most massive objects in the Kreutz system, the source or sources of the stream, the nature of the processes that govern the stream’s formation and evolution, as well as the period of time and the volume of space over which the activity has been continuing. To assist in solving these complex intertwined topics, in Part I of this investigation I examined the annual arrival rate variations of the Kreutz sungrazers in the stream, including the tendency toward swarming in both time and the longitude of the ascending node.

2. PERIHELION FRAGMENTATION

The two main populations of the Kreutz system, equivalent to Marsden’s (1967) original Subgroups I and II, still provide one of the fundamental dividing lines today, when the number of known members is orders of magnitude greater. Below I demonstrate that by paying attention to the two populations in the SOHO database as well as among the brightest objects, one gains new insights into the stream’s formation and evolution.

Even though Populations I and II are known to differ from each other greatly in a number of respects, the enormous disparities have generally been acknowledged and accepted with no comment, as if they were expected. The most obvious among these imbalances is the huge discrepancy in the arrival rates: even though different authors report different numbers, the Population I membership among the SOHO sungrazers does always greatly outnumber Population II. Recently, I have derived a ratio of 14:1 from a SOHO database for the years 1996 through mid-2010 that lists objects seen exclusively in the C2 coronagraph (Sekanina 2022a). This enormous ratio implies that the arrival rate of the SOHO sungrazers for one of the two populations is necessarily anomalous: either it is much too high for Population I or much too low for Population II.

Similarly disparate are the properties of the two populations’ brightest members and presumably the largest surviving masses of the Kreutz progenitor: the Great March Comet of 1843 (C/1843 D1), of Population I; and the Great September Comet of 1882 (C/1882 R1), of Population II. While they may have been about equally bright intrinsically before perihelion (when too few observations were made to be sure), the 1882 sungrazer was much brighter long after perihelion, apparently because of its near-perihelion splitting. By contrast, the 1843 sungrazer exhibited no signs of breakup and faded rapidly when receding from the Sun.

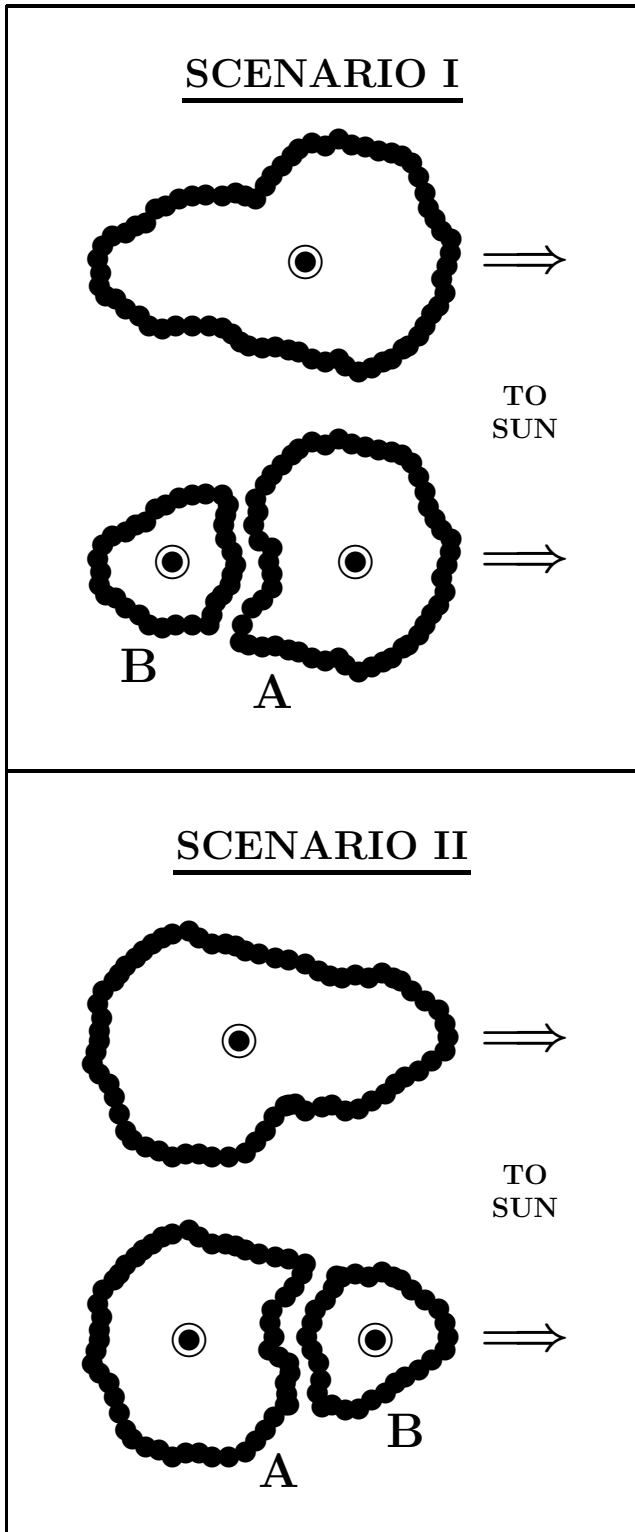


Figure 1. A sungrazer’s nucleus in close proximity of perihelion shortly before and after breaking up tidally into two uneven fragments. In Scenario I (top), it is the more sizable fragment A that begins its existence on the sunward side of the parent’s nucleus (to the right). It ends up in an orbit of shorter orbital period than the parent’s. On the other hand, the smaller fragment B, on the far side from the Sun, enters an orbit of longer orbital period than was the parent’s. In Scenario II, the positions of the two fragments are swapped and so are their future orbital periods. The circled disks are the centers of mass of the parent comet and the two fragments. (From Sekanina & Kracht 2022.)

2.1. Perihelion Breakup of the 1882 Sungrazer

As discussed later in this paper, the phenomenon of perihelion breakup, triggered presumably by the Sun’s tidal forces, is likely to be the initial stage of the process of formation of the stream of SOHO sungrazers. Using the well-known breakup of the Great September Comet of 1882, I will, in Section 2.3, point to a new implication of the differences between Populations I and II.

First of all, I employ a simple, but critically important rule on the orbital transformation, that Sekanina & Kracht (2022) used in their orbit-integration computations. The rule is illustrated in Figure 1: at the instant of breakup, the parent sungrazer and its center of mass, moving with a given orbital velocity, suddenly turn into two or more fragments, each with its own center of mass, but both/all still moving with the orbital velocity of the original body. The difference between the distances from the Sun of the centers of mass of the parent and each of the fragments makes the latter enter a new orbit with a different orbital period. The fragment whose center of mass is farther from the Sun than the parent’s ends up in an orbit of a longer period and vice versa. It is straightforward to show that the orbital period of a fragment, P_{frg} , is related¹ to the orbital period of the parent, P_{par} , by

$$P_{\text{frg}} = P_{\text{par}} \left(1 - \frac{2U_{\text{frg}}}{r_{\text{frg}}^2} P_{\text{par}}^{\frac{2}{3}} \right)^{-\frac{3}{2}}, \quad (1)$$

where r_{frg} is the heliocentric distance at fragmentation, U_{frg} is the difference between the heliocentric distances of the fragment’s and the parent’s centers of mass; U_{frg} is positive when the fragment is farther from the Sun than the parent. In Equation (1) both r_{frg} and U_{frg} must be in AU and P_{par} and P_{frg} in yr. The relation can also be written as

$$U_{\text{frg}} = \frac{1}{2} r_{\text{frg}}^2 \left(P_{\text{par}}^{-\frac{2}{3}} - P_{\text{frg}}^{-\frac{2}{3}} \right). \quad (2)$$

The minimum absolute value of U_{frg} for a given pair of periods P_{par} and P_{frg} is obviously reached at perihelion. Assuming that sungrazers could be tidally disrupted anywhere between perihelion and a point in the orbit of up to, say, $3.4 R_{\odot}$ from the Sun (crudely estimated from the Roche limit) and given that the perihelion distance of some sungrazers is as low as $1.1 R_{\odot}$, Equation (2) shows that the dimensions of sungrazers’ fragments could not be estimated from effects on the orbital period with accuracy much better than a factor of ten. In any case the differences between the orbital periods of the parent and a fragment (or between different fragments) provide information on the quantity of $U_{\text{frg}}/r_{\text{frg}}^2$.

Kreutz (1891) investigated the orbital motions of four fragments of the nucleus of the 1882 sungrazer in considerable detail. He called the fragments No. 1 through No. 4, although they are nowadays referred to usually as A through D. Although the number of observed fragments was at times greater, Kreutz was not able to collect enough data to compute satisfactory orbits for the additional ones.

¹ The only approximation used in the derivation of this expression is $r_{\text{frg}} + U_{\text{frg}} \doteq r_{\text{frg}}$, which for the Kreutz sungrazers involves typically an error on the order of 10^{-6} .

Table 1
Perihelion Fragmentation of Great September Comet of 1882 (C/1882 R1)

Parent comet ^a	Frag-ment	Orbital period (yr)		Differ-ence (yr)	$U_{\text{frg}}/r_{\text{frg}}^2$ wrt parent (AU ⁻¹)	U_{frg} for $r_{\text{frg}} = q$ (km)
		osculating	future			
C/1882 R1	A	671.3 ± 6.5	618	84	-0.000561	-5.04 ± 0.46
$q = 0.00775$ AU	B	771.8 ± 2.8	702	85	0.000000	0.00 ± 0.15
$P_{\text{par}} = 702$ yr	C	875.0 ± 4.4	787	63	+0.000464	+4.17 ± 0.25
	D	955.2 ± 8.9	850		+0.000758	+6.81 ± 0.38

Note.

^a Parent comet’s perihelion distance q and future orbital period (barycentric).

The osculating orbital periods derived by Kreutz for the fragments A through D are presented in column 3 of Table 1. Fragment B is assumed to be the primary, by far the most massive fragment, which after the perihelion-breakup event continued to move essentially in the orbit of the parent sungrazer, C/1882 R1.² Based on the computations by Sekanina & Chodas (2007), the corresponding future barycentric orbital periods are given in column 4, while column 5 shows the differences. The ratio of $U_{\text{frg}}/r_{\text{frg}}^2$, derived from Equation (2), is displayed in column 6. The last column provides the shift in the heliocentric distance of each fragment’s center of mass relative to the parent’s for fragmentation taking place at perihelion. Yes, a shift of mere 5 km in the radial position of the center of mass implies a change of 85 years in the fragment’s orbital period!

I used a method devised for other purposes in one of my recent papers (Sekanina 2021a) to check whether it is at all possible to satisfy a condition that B be located at the center of mass of the parent while the centers of mass of A, C, and D be distributed in line with the distances determined by their post-breakup orbital periods in Table 1. The method, based on the properties of a spheroid, shows that this indeed is possible. For a tidal event at perihelion, the condition is satisfied when the length of the spheroid is 18.7 km and the masses of the fragments are in the ratios of A : B : C : D = 0.27 : 0.46 : 0.16 : 0.11. The primary would thus retain almost 50 percent of the pre-breakup mass. It is likely that the method underestimates the mass of B. Given that r_{frg} could be up to twice the perihelion distance, the spheroid nucleus of the 1882 sungrazer before its perihelion breakup may have been up to about 75 km in length. In a previous paper (Sekanina 2002) I crudely estimated the comet’s nucleus to be about 50 km across. These dimensions would imply that the tidal fragmentation occurred at a heliocentric distance of $2.7 R_{\odot}$.

² Throughout this paper, Kreutz’s (1891) nonrelativistic set of orbital elements rather than Hufnagel’s (1919) relativistic set is used for fragment B of the 1882 sungrazer, because the latter is likely to be erroneous. Hufnagel’s numbers show that inclusion of the relativistic effect diminished the orbital period by 1.4 percent. However, Marsden’s (1967) orbit determination of comet Ikeya-Seki indicated that inclusion of the relativistic effect *increased* the orbital period by less than 0.2 percent. Also, his integration of Kreutz’s nonrelativistic orbit back to the 12th century implied the parent comet’s perihelion time in April 1138, which matched the parent sungrazer’s proposed time to within an incredible 0.04 percent of the orbital period! Integration of Hufnagel’s orbit, on the other hand, resulted in a meaningless date in November 1849.

2.2. Perihelion Breakup of the 1882 Sungrazer’s Parent Comet

Marsden’s (1967) proof that the sungrazers C/1882 R1 and C/1965 S1 were a single object on their way to the 12th century perihelion has motivated me to consider applying this procedure to their parent, recently identified as the Chinese Comet of 1138 reported in September of that year (Sekanina & Kracht 2022). The Great September Comet of 1882 should serve as the principal fragment. I have searched for additional fragments and found two potential ones. In Strom’s (2002) list of previously unrecognized Chinese daytime observations of “sun-comets”, one event is dated to April or May of 1792, reported from the Shandong Province. While it is by no means certain, or even probable, that this indeed was a Kreutz sungrazer, I count it in for the sake of argument.

The second candidate is comet X/1702 D1, which as 1702a was considered by Kreutz (1901). Even though the poor quality of the observations did not allow him to compute an orbit, his opinion was that the comet’s motion could better be fitted with the orbit of C/1882 R1 than C/1843 D1, and that the perihelion time, converted to TT, was close to February 15.0.

The potential perihelion-fragmentation products of the Chinese comet of 1138 are presented in Table 2, which is organized in a manner resembling that of Table 1. The reader will note that if the breakup took place at perihelion, the overall range of U_{frg} was about 12 km (implying a spheroid nearly 19 km in length) for the Great September Comet of 1882, but 16 km for its parent. In any case, the similarity between the numbers of U_{frg} for fragments A and C on the one hand and for 1792 and C/1965 S1 on the other hand is stunning. As it is by no means obvious that comet X/1702 D1 was actually a fragment of the Chinese comet of 1138, one similarly finds no reason why another fragment could not in due time follow comet Ikeya-Seki.

This argument does in turn tempt one to directly ask a highly contentious question: “*So what about the future?*” A potential follower of comet Ikeya-Seki in the chain would arrive at a time determined by its own value of U_{frg} . For example, at $r_{\text{frg}} = q$ a doubled Ikeya-Seki value, $U_{\text{frg}} = 8$ km, would lead to $P_{\text{frg}} = 927$ yr and a perihelion time in 2065. If, instead, U_{frg} for the next fragment were close to that for fragment D of the Great September Comet of 1882, it should arrive in 2032. Given the current low level of SOHO Population II activity, this possibility does not look likely.

Table 2
Perihelion Fragmentation of Chinese Comet of 1138, Parent of C/1882 R1 and C/1965 S1

Parent comet ^a	Fragment	Orbital period (yr)		Differ- ence (yr)	$U_{\text{frg}}/r_{\text{frg}}^2$ wrt parent (AU ⁻¹)	U_{frg} for $r_{\text{frg}} = q$ (km)
		osculating	baryc.			
Chinese Comet of 1138 $q = 0.008045$ AU $P_{\text{par}} = 744$ yr	X/1702 D1	564	90	-0.001235	-12.0
	1792 ^b	654	90	-0.000547	-5.3
	C/1882 R1	772 ± 3	744	83	0.000000	0.0
	C/1965 S1	827		+0.000415	+4.0

Notes.

^a Parent comet’s perihelion distance q and future orbital period (barycentric).

^b Sun-comet seen in April/May in Shandong Province; event recorded in Chinese annals (Strom 2002).

2.3. Presumed Perihelion Breakup of the Great Comet of 1106 (X/1106 C1)

From the limited results of available observations of the nuclear region made with modest telescopes of the time, such as the descriptions by C. Piazzzi Smyth at Cape (Warner 1980), the Great March Comet of 1843 displayed no obvious signs of breakup. In addition, no records exist about a bright Population I sungrazer at equivalent times, about 80 to 90 years before or following the 1843 spectacle.

Comets C/1880 C1 and C/1887 B1 would not do. They arrived at inappropriate times and C/1887 B1 was almost certainly a subfragment of C/1880 C1, which itself appeared to have been the product of an episode of nontidal fragmentation that took place at fairly large heliocentric distance (Sekanina 2021b). Besides, either object was much too small³ to represent a major fragment of such a magnificent comet as X/1106 C1 was.

Comet Pereyra (C/1963 R1) would fit sizewise, but it moved in a wrong orbit, as illustrated by Marsden’s (1989) difficulties with its motion. Also, the associated population is classified as a separate branch of Population I, with a distinct range of nodal longitudes (Sekanina 2021b), and the fragmentation history of comet Pereyra had apparently not been directly linked to the Great Comet of 1106, but to a presumed sungrazer of 1041 (Sekanina & Kracht 2022).

If the Great Comet of 1106 did not split at perihelion, why do we witness such an astonishingly prominent presence of Population I in the stream of SOHO sungrazers? A possible but rather shocking solution to this dilemma is provided by the expression $U_{\text{frg}}/r_{\text{frg}}^2$ in Equations (1) and (2). If the positions of the fragments’ centers of mass share similar patterns for the sungrazers of either population in that the values of U_{frg} are comparable, the substantially smaller perihelion distances of Population I objects cause that *the arrivals of these fragments should stretch* over time periods at least *twice as wide* as do the Population II sungrazers. It is likely that X/1106 C1 *did split*, but the fragments have been scattered too far apart to be easily recognized as such.

³ For example, Gould (1891) remarked that positional measurements of comet C/1880 C1, observed over a period of only two weeks after perihelion, “were rendered difficult by the lack of a nucleus or condensation in the head, which appeared like a cloud, elongated in the direction of the tail and of but slightly greater brilliancy.” This description is strongly reminiscent of the words depicting cometary nuclei in the process of disintegration.

This disparity shows up when I apply the conditions for fragments A and B of C/1882 R1 from Table 1 (referred to as Scenario Y⁻) and for comets 1792 and C/1882 R1 as fragments of comet 1138 from Table 2 (Scenario Z⁻) to an equivalent episode of perihelion fragmentation experienced by X/1106 C1 to see when the 1843 sungrazer’s sibling that preceded it should have arrived. I next apply the conditions for fragments B and C of C/1882 R1 from Table 1 (Scenario Y⁺) and sungrazers C/1882 R1 vs C/1965 S1 from Table 2 (Scenario Z⁺) to an equivalent fragmentation event of X/1106 C1 to see when the 1843 sungrazer’s sibling that follows it may arrive.

The results in Table 3 confirm what was said above, yet they do offer a surprise. If the fragmentation constants derived for the Population II sungrazers apply to X/1106 C1 as well, the fragment preceding C/1843 D1 should have been C/1668 E1, believed by some in the mid-19th century to have been the 1843 sungrazer’s previous return to the Sun (e.g., Henderson 1843)! A map of the 1668 comet’s path as seen from Goa, India, was examined by Kreutz (1901). He concluded that the comet moved in the orbital plane of C/1843 D1 and for an appropriately selected perihelion time the elements did not contradict the observations; comparison with C/1882 R1 was less satisfactory. Marsden (1967) did include the comet of 1668 among his eight Kreutz objects.

The younger generation of comet enthusiasts might be interested to learn that *this procedure predicts* the appearance of a naked-eye Population I sungrazer within the next 50 years or so — the X/1106 C1 fragment that follows C/1843 D1. I noted in Section 2.2 that a major member of Population II, a sibling of comet Ikeya-Seki, is also expected to arrive at about the same time.

Table 3

Potential Evidence for Perihelion Fragmentation of X/1106 C1 from Fragmentation Constants for Population II Sungrazers

Parent comet	Scenario	Orbital period (yr)	Differ-ence (yr)	Arriving in year or as comet	Candidate comet
X/1106 C1 $q = 0.005342$ AU $P_{\text{par}} = 737$ yr	Y ⁻	565	172	1671	C/1668 E1
		737	219	C/1843 D1
	Y ⁺	956		2062	??
	Z ⁻	559	178	1665	C/1668 E1
		737	209	C/1843 D1
	Z ⁺	946		2052	??

Approximately equivalent timelines for arrivals of new naked-eye members of Populations I and II clearly contradict the uneven contributions to the stream of SOHO sungrazers. However, the dominance of Population I could be interpreted in various ways. Besides the one to regard it as supporting evidence for an “imminent” arrival of a spectacular member of Population I, one could take an opposite view and argue that the overwhelming preponderance of Population I among the SOHO sungrazers represents the debris of the disintegrated naked-eye object that we have been waiting for in vain. A problem with this view is that if a sungrazer kilometers across fell apart, the debris stream should be orders of magnitude more plentiful. The problem is further complicated by the existence of temporally limited enhancements of dwarf comets, as noted in Part I.

In a striking example, a burst of SOHO/STEREO sungrazers reaching magnitude 3 or brighter at maximum light was reported by Sekanina & Kracht (2013). The period of time covered by the study was 2004–2013, but the highly elevated arrival rates were restricted to a few years centered on the peak of 4.6 objects per year at the end of 2010. This happened to be almost exactly one year before the appearance of comet Lovejoy (C/2011 W3), which had no direct association with the burst consisting exclusively of Population I members. By 2013 the rate was back to normal, 1–2 comets brighter than magnitude 3 per year.

Because of uncertainties beyond the limits of the applied procedure, the prospects for the arrival of a brilliant Population I sungrazer in a much nearer future than ~ 40 or so years from now cannot be ruled out. Overall, it appears to be more likely than the early arrival of a naked-eye Population II sungrazer.

2.4. Peculiar Kreutz Sungrazers

One may be tempted to recognize two kinds of a Kreutz sungrazer: its nucleus is large enough to survive its return to the Sun either essentially intact or split into two or more fragments; or it is too small to survive and perishes just before perihelion.

Comet Lovejoy defied either scenario. This sungrazer, discovered before perihelion from the ground but observed by a number of space observatories throughout the perihelion arc of its sungrazing orbit and starting as early as 1 day after perihelion again from the ground, did survive perihelion and began to immediately develop its new dust tail. However, on a ground-based image taken 3.4 days after perihelion, a narrow streamer at least 200,000 km long showed up, suggesting that the comet suffered a modest outburst. Twenty-four hours later, the object’s morphology changed radically, its nuclear condensation *very suddenly* disappearing. Examination of systematic ground-based imaging observations of the new straight, ribbon-like “spine” or trail of material, which replaced the ordinary dust tail, allowed us to determine that the disintegration process commenced as early as 1.6 ± 0.2 days after perihelion (Sekanina & Chodas 2012). We estimated that the nucleus was about 400 meters across upon approach to the Sun.

In retrospect, comet Lovejoy was not the only Kreutz sungrazer that *survived perihelion but not the entire perihelion return*. The strange comet C/1887 B1, observed as a headless tail over a period of 10 days starting 8 days

after perihelion, must have been subjected to the same type of catastrophic event 0.24 ± 0.03 day after perihelion (Sekanina 1984), suggesting that the initial dimensions of its nucleus were smaller than Lovejoy’s. I suspect that C/1880 C1 was close to experiencing the Lovejoy-type event, avoiding it just narrowly.

Another potential member of this exceptional category of Kreutz sungrazers, comet du Toit (C/1945 X1), does not as yet contribute to our knowledge of this type of events, but a comprehensive examination of the relevant Boyden plates — now that their digitized version has become available — could offer new information. The comet was last photographed about 13 days before perihelion and not seen ever since. Unless some positive evidence does show up in the future, this object could rank as a dwarf Kreutz comet (Sekanina & Kracht 2015a), a view that Seargent (2009) also appears to be in favor of. However, the comet was then exceptionally bright before perihelion, an anomaly that needs to be explained.

2.5. Sunlight Striking An Eroding Sungrazer Near Perihelion

An important part of interaction with the Sun near perihelion is the amount of radiation that is incident on an eroding sungrazer’s surface. It is standard to assume that the solar flux drops with increasing heliocentric distance r at a rate of $f_{\odot}(r) = R_{\odot}^2/r^2$, where R_{\odot} is the radius of the Sun’s photosphere. This point-source approximation is fine as long as $r \gg R_{\odot}$, but does not apply near the Sun, when the radiation reaching the sungrazer’s surface comes from only a small part of the Sun’s surface, which however is much closer to the sungrazer than r .

The correct expression for f_{\odot} is derived by following a schematic picture in Figure 2. The area of the Sun’s photosphere, from which the radiation reaches the sungrazer, is the shaded cap centered on the sungrazer’s subsolar point, whose distance from the comet is $r - R_{\odot}$. The radiation from a sum of infinitesimal areas of width $R_{\odot} d\phi$, like the one projected in the figure as a rhombus, integrated along the dotted circle of radius $R_{\odot} \sin \phi$ on the Sun’s surface and at a distance ρ from the comet, amounts to $2\pi R_{\odot}^2 \cos(\phi + \psi) \sin \phi d\phi / \rho^2$, where $\phi + \psi$ is the angle that the normal to the radiation area subtends with the direction to the sungrazer. Normalizing and

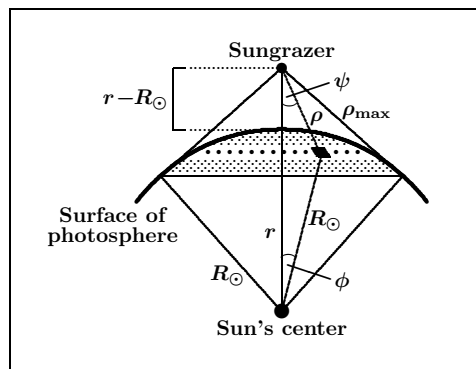


Figure 2. Sunlight incident on a sungrazer in a close-up. Only the radiation from the dotted area of the photosphere reaches the comet. The rhombus shows an infinitesimal area on the Sun, whose distance from the sungrazer is ρ and the angles from the Sun-comet line are ϕ and ψ , reckoned at their centers, respectively.

Table 4
Expressions $A = 2\left[1 - \sqrt{1 - (R_\odot/r)^2}\right]$, $B = (R_\odot/r)^2$, and Their Ratio C As Function of Heliocentric Distance r

Distance from Sun, r (AU)	$A = 2\left[1 - \sqrt{1 - \left(\frac{R_\odot}{r}\right)^2}\right]$	$B = \left(\frac{R_\odot}{r}\right)^2$	$C = \frac{A}{B}$	Distance from Sun, r (R_\odot)	$A = 2\left[1 - \sqrt{1 - \left(\frac{R_\odot}{r}\right)^2}\right]$	$B = \left(\frac{R_\odot}{r}\right)^2$	$C = \frac{A}{B}$
1.00	0.0000216	0.0000216	1.0000	2.0	0.26795	0.25000	1.0718
0.50	0.0000865	0.0000865	1.0000	1.9	0.29942	0.27701	1.0809
0.20	0.0005406 ₄	0.0005405 ₆	1.0001	1.8	0.33704	0.30864	1.0920
0.10	0.0021634	0.0021623	1.0005	1.7	0.38262	0.34602	1.1058
0.05	0.0086678	0.0086490	1.0022	1.6	0.43875	0.39063	1.1232
0.03	0.0241711	0.0240250	1.0061	1.5	0.50929	0.44444	1.1459
0.02	0.0548072	0.0540563	1.0139	1.4	0.60029	0.51020	1.1766
0.015	0.0985269	0.0961000	1.0253	1.3	0.72206	0.59172	1.2203
0.01	0.2293786	0.2162250	1.0608	1.25	0.80000	0.64000	1.2500
0.008	0.3725499	0.3378516	1.1027	1.2	0.89446	0.69444	1.2880
0.006	0.7360775	0.6006250	1.2255	1.15	1.01236	0.75614	1.3389
0.0055	0.9319052	0.7147934	1.3027	1.1	1.16680	0.82645	1.4118
0.005	1.2648840	0.8649000	1.4625	1.05	1.39018	0.90703	1.5327
0.0048	1.5039216	0.9384766	1.6025	1.0	2.00000	1.00000	2.0000

integrating over all relevant angles ϕ , one has

$$f_\odot(r) = 2R_\odot^2 \int_0^{\arccos(R_\odot/r)} \frac{\cos(\phi + \psi) \sin \phi}{\rho^2} d\phi, \quad (3)$$

where

$$\begin{aligned} \rho \sin \psi &= R_\odot \sin \phi, \\ \rho \cos \psi &= r - R_\odot \cos \phi, \end{aligned} \quad (4)$$

so that

$$\cos(\phi + \psi) = \frac{r \cos \phi - R_\odot}{(r^2 + R_\odot^2 - 2rR_\odot \cos \phi)^{\frac{1}{2}}}. \quad (5)$$

Inserting this expression into Equation (3) one gets, after substituting $\cos \phi = x$, the result:

$$\begin{aligned} f_\odot(r) &= 2R_\odot^2 \int_{R_\odot/r}^1 \frac{rx - R_\odot}{(r^2 + R_\odot^2 - 2rR_\odot x)^{\frac{3}{2}}} dx \\ &= 2 \left[1 - \sqrt{1 - \left(\frac{R_\odot}{r}\right)^2} \right]. \end{aligned} \quad (6)$$

As expected,

$$\lim_{r \gg R_\odot} f_\odot(r) = \left(\frac{R_\odot}{r}\right)^2. \quad (7)$$

The significance of the correct procedure is apparent from Table 4, in which the accurate expression, referred to as A , is compared with the approximate one, B , in a wide range of heliocentric distances. It turns out that the amount of solar radiation reaching the surface of a sungrazer is always *higher* than the inverse square power law suggests. However, while the difference is still only a fraction of 1 percent at a distance as small as 0.03 AU from the Sun, at 0.01 AU it already reaches 6 percent. Table 4 shows that the magnitude of the effect increases progressively at close proximity of the Sun but stays smaller than a factor of two in any sungrazing orbit.

To what extent does his effect influence the sungrazers' rate of erosion? A straightforward answer can readily be provided by illustrating the progressing sublimation of a column of water ice integrated along a sungrazing parabolic orbit. Let $\dot{Z}(r)$ be the rate of sublimation (reckoned in a number of molecules per cm^2 per second) from a sphere of water ice at r , as determined from a standard, surface-averaged energy balance equation using an inverse square power-law approximation (e.g., Delsemme & Miller 1971). If m is the mass of a water molecule and $\rho_0 = 0.5 \text{ g cm}^{-3}$ a bulk density of the sphere, a layer of ice lost by the sphere between aphelion and time $t - t_\pi$, measured from perihelion, has a thickness τ equaling

$$\tau = \int_{-\infty}^{t-t_\pi} \frac{m\dot{Z}(r)}{\rho_0} dt = \frac{\sqrt{2}mq^{\frac{3}{2}}}{\rho_0 k_0} \int_{-\frac{1}{2}\pi}^{\frac{1}{2}u} \frac{\dot{Z}(r)}{\cos^4 \frac{1}{2}u} d(\frac{1}{2}u), \quad (8)$$

where u is the true anomaly at time t and heliocentric distance r , and k_0 is the Gaussian gravitational constant. The sublimation rates $\dot{Z}(r)$, derived from the standard inverse square power law, underestimate the thickness of the eroded layer of ice when inserted into Equation (8). To account approximately for the effect expressed by Equation (6) and thus obtain a corrected thickness of the eroded ice layer, \hat{r} , one needs in each integration step in Equation (8) to substitute \hat{r} for r ,

$$\hat{r} = \frac{R_\odot}{\sqrt{2}} \left[1 - \sqrt{1 - \left(\frac{R_\odot}{r}\right)^2} \right]^{-\frac{1}{2}}, \quad (9)$$

and replace $\dot{Z}(r)$ with $\dot{Z}(\hat{r})$. The integration limits remain unaffected by this change.

The increasing erosion of the layer on the surface of a water-ice sphere along the preperihelion branch of a sungrazing orbit is for three perihelion distances between $1.04 R_\odot$ and $1.6 R_\odot$ displayed in Table 5. The numbers are near a lower end of the usual range, as they apply to the surface averaged case of the sublimation regime, the so-called rapidly rotating comet. The approximate, widely used model based on the inverse square power law

Table 5
Layers of Water Ice Eroded Under Inverse Square Power Law, τ , and Under Law (6), $\hat{\tau}$, Along Preperihelion Branch of Sungrazing Orbit from Aphelion to Given Heliocentric Distance

Distance from Sun, r (R_{\odot})	Perihelion distance $1.6 R_{\odot}$				Perihelion distance $1.2 R_{\odot}$				Perihelion distance $1.04 R_{\odot}$			
	τ (m)	$\hat{\tau}$ (m)	Diff. (percent)	$t-t_{\pi}$ (hr)	τ (m)	$\hat{\tau}$ (m)	Diff. (percent)	$t-t_{\pi}$ (hr)	τ (m)	$\hat{\tau}$ (m)	Diff. (percent)	$t-t_{\pi}$ (hr)
30	3.0	3.0	0.0	-36.9	3.0	3.0	0.0	-36.3	3.0	3.0	0.0	-36.0
20	4.1	4.1	0.0	-20.8	4.1	4.1	0.0	-20.3	4.1	4.1	0.0	-20.0
15	5.1	5.1	0.0	-13.9	5.1	5.1	0.0	-13.5	5.1	5.1	0.0	-13.3
10	7.0	7.0	0.1	-8.0	6.9	6.9	0.1	-7.7	6.9	6.9	0.1	-7.5
8	8.2	8.2	0.1	-5.9	8.1	8.1	0.1	-5.7	8.1	8.1	0.1	-5.5
6	10.2	10.2	0.2	-4.0	10.1	10.1	0.2	-3.8	10.0	10.0	0.2	-3.7
4	14.0	14.1	0.5	-2.3	13.6	13.7	0.5	-2.2	13.5	13.6	0.5	-2.2
3	17.8	18.0	0.9	-1.5	17.1	17.2	0.9	-1.5	16.8	16.9	0.8	-1.5
2.5	21.0	21.2	1.3	-1.1	19.8	20.0	1.3	-1.2	19.4	19.6	1.3	-1.2
2	26.4	27.0	2.3	-0.7	24.0	24.5	2.1	-0.8	23.3	23.7	2.1	-0.8
1.8	30.2	31.1	3.2	-0.5	26.4	27.1	2.8	-0.7	25.5	26.2	2.7	-0.7
1.6	40.8	43.1	5.5	0.0	29.7	30.8	3.7	-0.5	28.4	29.4	3.6	-0.6
1.4	34.7	36.7	5.5	-0.4	32.4	34.0	5.1	-0.5
1.3	38.7	41.5	7.2	-0.2	35.1	37.3	6.4	-0.4
1.2	49.4	55.2	11.8	0.0	38.8	42.0	8.4	-0.3
1.1	44.4	49.8	12.2	-0.2
1.06	48.5	55.9	15.3	-0.1
1.04	54.3	65.1	20.0	0.0

for the incident solar radiation, yielding the thickness τ , is compared with the preferred model governed by Equation (6), increasing the thickness to $\hat{\tau}$. The relative difference is given in percent, showing that it could reach up to 20 percent only in orbits that penetrate very deep, nearly to the very surface of the photosphere.

Most SOHO Kreutz sungrazers disintegrate 6–8 hr before perihelion (measured by extrapolation along the fitted parabolic orbit — see Part I of this investigation). Table 5 shows that by that time a layer of water ice 7–8 meters thick would erode. Thus, an icy boulder 15 meters in diameter would by then sublimate away completely. The smallest Kreutz sungrazers detected by SOHO are believed to be 5–10 meters in diameter at the time they begin their final approach (e.g., Battams & Knight 2017).

3. MODELING THE FRAGMENTATION PROCESS

Failure of the SOHO Kreutz sungrazers to survive perihelion is powerful evidence for an argument that the dimensions of the objects that did survive as products of a parent comet’s perihelion breakup to begin their journey about the Sun must have been much larger. Subjected to the process of *cascading fragmentation*, many of them ended up a revolution later as boulders in an estimated meter-size range. The consensus is that the stream contains even larger numbers of still smaller fragments. Discovery of more than a dozen sungrazers with the camera on board the Parker Solar Probe, some not seen by SOHO, appears to be the case in point.

In the following, I describe the assumptions and constraints I employ to incorporate cascading fragmentation in the computations. But first I address a hypothetical yet key issue: *How an arrival-rate curve of a stream of SOHO-like meter-sized boulders would look like in the absence of fragmentation, that is, if the boulders were directly stripped from the surface of a parent sungrazer at perihelion and miraculously survived until next perihelion?*

3.1. Stream’s Hypothetical Fragmentation-Free Model

Let a massive sungrazer shed an enormous number of boulders at the time of perihelion passage. Allowed to survive, they end up in orbits whose periods are governed by Equation (1) and return to perihelion at different times as a stream, presumably similar to that observed in the coronagraphs on board SOHO. What would be a range of the boulders’ orbital periods and the stream’s timeline upon return to perihelion?

I approximate the shape of the sungrazer’s nucleus by a prolate spheroid and assume that at the time the boulders were removed, the long axis of the nucleus was aligned with the Sun direction. Let U_{frg} be a distance from the center of the spheroidal nucleus along the Sun-comet line, reckoned positive away from the Sun, and let the mass of the fraction of the boulders removed between the radial distances of U_{frg} and $U_{\text{frg}} + dU_{\text{frg}}$ be dm and their number, $d\mathcal{N}$, proportional to dm .

Elsewhere I showed (Sekanina 2021a) that the normalized volume (or mass), $\mathfrak{S}(\eta)$, of a prolate spheroid’s cap of a normalized height, η , measured in units of the spheroid’s long diameter, \mathcal{D} , from its sunward pole to a plane perpendicular to the long axis equals

$$\mathfrak{S}(\eta) = 3\eta^2(1 - \frac{2}{3}\eta). \quad (10)$$

For $\eta = 1$ this formula gives $\mathfrak{S} = 1$, confirming that the spheroid cap’s height has indeed been normalized. Similarly, as expected, $\eta = \frac{1}{2}$ implies $\mathfrak{S} = \frac{1}{2}$. The proportionality $d\mathcal{N} \sim dm$ now becomes

$$d\mathcal{N} = \mathcal{N}_0 d\mathfrak{S} = 6\mathcal{N}_0\eta(1-\eta) d\eta, \quad (11)$$

where \mathcal{N}_0 equals the total number of the boulders that were stripped from the sungrazer’s surface. Replacing the normalized distance of a boulder’s position from the sunward end of the prolate-spheroidal nucleus, η , with its normalized distance from the nucleus’ center of mass,

v , along the radial axis, one has

$$v = \eta - \frac{1}{2} \quad (12)$$

and Equation (11) becomes

$$d\mathcal{N} = \frac{3}{2}\mathcal{N}_0(1 - v^2) dv. \quad (13)$$

Each fragment is handled as a dimensionless point, whose normalized radial deviation from the heliocentric distance of the parent's center of mass, r_{frg} , is $v = U_{\text{frg}}/\mathcal{D}$, where $-\frac{1}{2} \leq v \leq +\frac{1}{2}$. Since from Equation (2)

$$dU_{\text{frg}} = \frac{1}{3}r_{\text{frg}}^2 P_{\text{frg}}^{-\frac{5}{3}} dP_{\text{frg}}, \quad (14)$$

and $\mathcal{D} dv = dU_{\text{frg}}$, I find by inserting from Equations (2) and (14) into Equation (13):

$$\dot{\mathcal{N}}(t) = \frac{1}{2}\mathcal{N}_0\chi P_{\text{frg}}^{-\frac{5}{3}} \left[1 - \chi^2 \left(P_{\text{par}}^{-\frac{2}{3}} - P_{\text{frg}}^{-\frac{2}{3}} \right)^2 \right], \quad (15)$$

where $\dot{\mathcal{N}}(t) = d\mathcal{N}/dt = d\mathcal{N}/dP_{\text{frg}}$, $t = t_\pi + P_{\text{frg}}$, t_π is the time of perihelion, when the boulders were removed, and χ (in AU) equals

$$\chi = \frac{r_{\text{frg}}^2}{\mathcal{D}}. \quad (16)$$

Equation (15) serves to determine the total number of boulders, \mathcal{N}_0 , from their observed annual arrival rate, $\dot{\mathcal{N}}(t_{\text{obs}})$. The orbital period of the observed boulders is $P_{\text{frg}} = P_{\text{obs}} = t_{\text{obs}} - t_\pi$, while the sungrazer itself returns at a time $t_{\text{par}} = t_\pi + P_{\text{par}}$.

The annual arrival rate $\dot{\mathcal{N}}(t)$ varies with time, depending on the distance U_{frg} of an element of the surface from which the boulders were stripped ($-\frac{1}{2}\mathcal{D} \leq U_{\text{frg}} \leq +\frac{1}{2}\mathcal{D}$). The earliest ones arrive at their perihelion well before does the returning sungrazer, at time $t_{\text{min}} = t_\pi + P_{\text{min}}$, where

$$P_{\text{min}} = P_{\text{par}} \left(1 + \frac{1}{\chi} P_{\text{par}}^{\frac{2}{3}} \right)^{-\frac{3}{2}}. \quad (17)$$

On the other hand, the last boulders arrive long after the returning sungrazer, at time $t_{\text{max}} = t_\pi + P_{\text{max}}$, where

$$P_{\text{max}} = P_{\text{par}} \left(1 - \frac{1}{\chi} P_{\text{par}}^{\frac{2}{3}} \right)^{-\frac{3}{2}}. \quad (18)$$

This equation makes sense only when

$$P_{\text{par}} < \chi^{\frac{3}{2}}. \quad (19)$$

If P_{par} does not satisfy this condition, some of the boulders get into hyperbolic orbits, ending up as interstellar objects.

The annual arrival rate $\dot{\mathcal{N}}(t)$ reaches a maximum at time $t_{\text{peak}} = t_\pi + P_{\text{peak}}$, where

$$P_{\text{peak}} = \frac{27\sqrt{7}}{49} P_{\text{par}} \left(1 + \frac{2}{7} \sqrt{1 + \Phi} \right)^{-\frac{3}{2}} \quad (20)$$

and

$$\Phi = \frac{45}{4\chi^2} P_{\text{par}}^{\frac{4}{3}}. \quad (21)$$

Because $\Phi > 0$, it is always $P_{\text{peak}} < P_{\text{par}}$ and $\dot{\mathcal{N}}$ reaches its peak before the parent sungrazer returns to perihelion.

The peak rate $\dot{\mathcal{N}}_{\text{peak}} = \dot{\mathcal{N}}(t_{\text{peak}})$ equals

$$\begin{aligned} \dot{\mathcal{N}}_{\text{peak}} &= \frac{1}{2} \left(\frac{\sqrt{7}}{3} \right)^5 \mathcal{N}_0 \chi P_{\text{par}}^{-\frac{5}{3}} \left(1 + \frac{2}{7} \sqrt{1 + \Phi} \right)^{\frac{5}{2}} \\ &\quad \times \left[1 - \frac{5}{9\Phi} \left(\sqrt{1 + \Phi} - 1 \right)^2 \right]. \end{aligned} \quad (22)$$

This hypothetical, fragmentation-free model predicts the rate of perihelion arrival of boulders as a function of time via Equation (15), in terms of the orbital period, a measure of the location of their removal from the surface of the parent sungrazer. Since no consideration has been given to the possibility that any of the initially stripped chunks could further fragment along the orbit, their total number remains constant.

For the sake of curiosity, the curve of the arrival rate of Population I boulders is in this unrealistic scenario displayed in Figure 3. The assumptions are that the boulders were stripped from the parent comet X/1106 C1 at perihelion, $r_{\text{frg}} = q$; that the length of its nucleus along the Sun-comet line was $\mathcal{D} = 50 \text{ km} = 0.334 \times 10^{-6} \text{ AU}$; and that an observed arrival rate was $\dot{\mathcal{N}}(t_{\text{obs}}) = 100 \text{ yr}^{-1}$ at $t_{\text{obs}} = 2010$, when $P_{\text{frg}} = 904 \text{ yr}$. The parameters of the parent sungrazer, which returned to perihelion as the Great March Comet of 1843, are taken from Table 3.

The results of this numerical exercise are most interesting. The earliest returning boulders, stripped from the sunward end of the nuclear surface, would never get beyond 84 AU from the Sun and would have reached perihelion in 1376 (period $P_{\text{min}} = 270 \text{ yr}$); the last ones, from the antisunward end, would not return for nearly 80,000 yr ($P_{\text{max}} = 77,100 \text{ yr}$), moving in orbits reaching 3600 AU from the Sun at aphelion! This enormous range of arrival times is a result of the large assumed dimensions of the comet's nucleus along the Sun-comet line at the time of boulder removal. If the length of the nucleus made an angle of 45° with the Sun-comet line, the periods would be restricted to a much tighter range from 342 yr to 3860 yr.

Because the arrival-rate curve has an extended tail toward the long periods, the stream would effectively be limited to just a few thousand years anyway; the arrival rates at later times would be extremely low. The curve in Figure 3 displays a sharp peak near the year 1500, almost 400 yr after perihelion, when the arrival rate would reach nearly three times the rate in 2010, followed by a gradual drop. In the year 3100 the rate would be only 20 percent of the one in 2010. The total number of boulders stripped from the surface of X/1106 C1 would amount to almost exactly 200,000.

3.2. Seeds for Cascading Fragmentation

A straightforward manner to incorporate the process of cascading fragmentation into a model for the stream of the SOHO Kreutz sungrazers is to begin with a seed object that breaks up into two equal fragments of the first generation, each of which subsequently breaks up into two equal fragments of the second generation, etc. If the mass of the seed object is \mathcal{M}_0 , the mass of each fragment of the first generation is $\mathcal{M}_1 = \frac{1}{2}\mathcal{M}_0$, etc., and the mass of each fragment of an arbitrary k -th generation, is

$$\mathcal{M}_k = \left(\frac{1}{2} \right)^k \mathcal{M}_0. \quad (23)$$

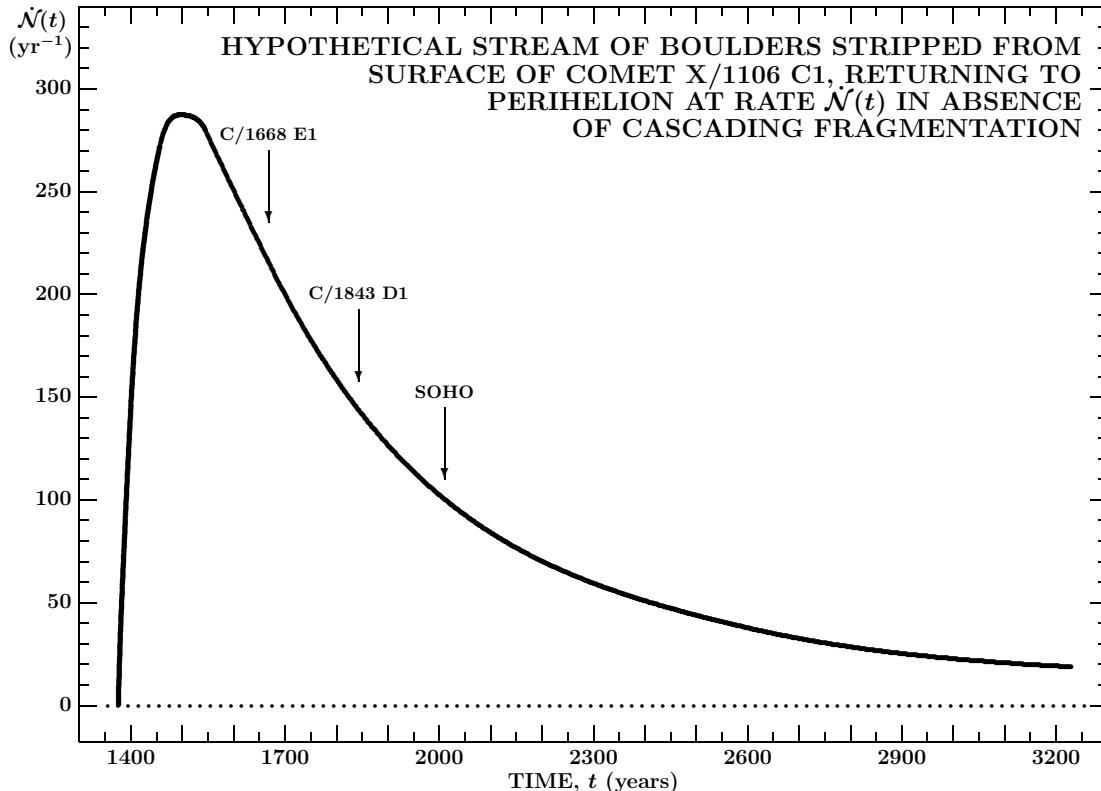


Figure 3. Curve of arrival rates of Population I boulders in a hypothetical case of absence of cascading fragmentation. The boulders are assumed to have directly been stripped from the surface of a 50-km long nucleus of comet X/1106 C1, ending up in independent orbits determined by their location and surviving their motion through the Sun’s corona to return back to perihelion. Note the sharp peak in the arrival rate near the year 1500. An arrival rate of 100 yr^{-1} in 2010 requires that a total of 200,000 boulders be removed. The time of the SOHO operations as well as the perihelion times of C/1843 D1 and C/1668 E1 are shown for reference.

Based on evidence offered by observations of the massive Kreutz sungrazers, discussed in Section 2, a more realistic scenario emerges that tidal splitting of a single parent in close proximity of perihelion gives rise in general to a multitude of seed objects. The implication is that instead of one source, cascading fragmentation should begin from several discrete sources that rapidly spread over time. However, regardless of the number of seeds, the age of a SOHO-imaged fragment seen to disintegrate suddenly upon return to perihelion is known with high accuracy, once the identity of the parent and the time of its tidal fragmentation, essentially equal to the perihelion time, are available.

3.3. Breakup by Rotation Instability: Spin-up and Separation Velocity

Strong observational evidence suggests that, subsequent to tidal splitting of the parent sungrazer, the seed objects and their fragments continue to fracture throughout the orbit. Although the disruption mechanism is not known with certainty and a variety of potential causes for splitting of comets has over the years been proposed (e.g., Whipple & Stefanik 1966; Boehnhardt 2002), rotational instability (breakup by runaway spin-up) has recently become the primary suspect as a result of torques exerted by anisotropic outgassing (e.g., Jewitt 2021, 2022; Ye et al. 2021).

To get insight into a spin-up scenario, I approximate an irregularly-shaped object by two equal hemispheres

attached to one another, each half having its own center of mass. If the radius equals $\mathfrak{R}_{\text{frg}}$, the distance between the two centers of mass is $2\alpha\mathfrak{R}_{\text{frg}}$, where $\alpha \simeq 0.35$. Let the hemispheres rotate with a period of P_{rot} . The rotation velocity of the center of mass of each is $2\pi\alpha\mathfrak{R}_{\text{frg}}/P_{\text{rot}}$ and the outward acceleration due to the centrifugal force amounts to $4\pi^2\alpha\mathfrak{R}_{\text{frg}}/P_{\text{rot}}^2$. If ρ_{frg} is the bulk density, the mass of each hemisphere comes to $\frac{2}{3}\pi\rho_{\text{frg}}\mathfrak{R}_{\text{frg}}^3$ and the hemispheres are pulled together gravitationally by a force equal to $\frac{1}{9}\pi^2G\rho_{\text{frg}}^2\mathfrak{R}_{\text{frg}}^4/\alpha^2$, where G is the universal constant of gravitation. The force generated by the rotation amounts to $\frac{16}{3}\pi^3\alpha\rho_{\text{frg}}\mathfrak{R}_{\text{frg}}^4/P_{\text{rot}}^2$ and acts in the opposite direction, aiming to separate the hemispheres from one another along their joint surface. I let the hemispheres spin up, until their tensile strength, σ_{T} , is overcome. The pull per unit surface area, $\pi\mathfrak{R}_{\text{frg}}^2$, that exceeds the limit is

$$\frac{16}{3}\pi^2\alpha\rho_{\text{frg}}\frac{\mathfrak{R}_{\text{frg}}^2}{P_{\text{rot}}^2} - \frac{1}{9}\pi G\rho_{\text{frg}}^2\frac{\mathfrak{R}_{\text{frg}}^2}{\alpha^2} > \sigma_{\text{T}}. \quad (24)$$

The condition for P_{rot} becomes

$$P_{\text{rot}} < 4\pi\mathfrak{R}_{\text{frg}}\sqrt{\frac{\alpha\rho_{\text{frg}}}{3\sigma_{\text{T}}}\frac{1}{\sqrt{1+\kappa}}}, \quad (25)$$

where

$$\kappa = \frac{1}{9}\pi G\rho_{\text{frg}}^2\frac{\mathfrak{R}_{\text{frg}}^2}{\alpha^2\sigma_{\text{T}}}. \quad (26)$$

When the hemispheres break apart, the separation ve-

locity of each center of mass, v_{sep} , amounts to

$$v_{\text{sep}} = \frac{2\pi\alpha\mathfrak{R}_{\text{frg}}}{P_{\text{rot}}} > \sqrt{\frac{3\alpha\sigma_{\text{T}}}{4\rho_{\text{frg}}}}\sqrt{1+\kappa}. \quad (27)$$

Should $\kappa \ll 1$, a solution that satisfies the condition of hemispheric separation implies v_{sep} whose lower limit depends on the fragment's tensile strength and bulk density but not on its size. Of course, it is the lower limit of v_{sep} that counts because that is when the separation begins. For a bulk density of $\rho_{\text{frg}} = 0.5 \text{ g cm}^{-3}$, κ equals

$$\kappa = 0.000048 \frac{\mathfrak{R}_{\text{frg}}^2}{\sigma_{\text{T}}}, \quad (28)$$

where $\mathfrak{R}_{\text{frg}}$ is in meters and σ_{T} in pascals.

It is possible to investigate the maximum possible size $\mathfrak{R}_{\text{frg}}$ for which v_{sep} stays within required limits of its value for $\kappa = 0$. The maximum size refers to the seed objects, with which cascading fragmentation begins, so this exercise inquires about how large the seed objects would have to be to satisfy the condition (27) within any particular limit. As an example, suppose I do not want v_{sep} to vary by more than 10 percent of the magnitude given by $\kappa = 0$. In this case the radius of the seed object, $\mathfrak{R}_{\text{seed}}$, would have to be such that $\sqrt{1+\kappa_{\text{seed}}} = 1.1$ and therefore $\kappa_{\text{seed}} = 0.21$. From Equation (26) this radius is equal to

$$\mathfrak{R}_{\text{seed}} = \frac{3\alpha}{\rho_{\text{frg}}} \sqrt{\frac{\kappa_{\text{seed}} \sigma_{\text{T}}}{\pi G}}. \quad (29)$$

Now, at spin periods exceeding $3.3 \rho_{\text{frg}}^{-\frac{1}{2}}$ hr solid bodies do not break rotationally even if their tensile strength is nil (e.g., Jewitt 1997).⁴ At a bulk density of 0.5 g cm^{-3} this critical spin period equals $P_{\text{crit}} = 4.67 \text{ hr}$. In the search for the maximum dimensions of the seeds that would satisfy the condition (27) (with $\kappa = \kappa_{\text{seed}}$), one obviously should require that at the same time their radius be smaller than the critical value $\mathfrak{R}_{\text{crit}}$, given by a condition⁵

$$v_{\text{sep}} = \frac{2\pi\alpha\mathfrak{R}_{\text{crit}}}{P_{\text{crit}}}, \quad (30)$$

that is,

$$\mathfrak{R}_{\text{crit}} = \frac{P_{\text{crit}}}{4\pi} \sqrt{\frac{3\sigma_{\text{T}}}{\alpha\rho_{\text{frg}}}}\sqrt{1+\kappa_{\text{peak}}}. \quad (31)$$

For the ratio I find, again with $\rho_{\text{frg}} = 0.5 \text{ g cm}^{-3}$

$$\frac{\mathfrak{R}_{\text{seed}}}{\mathfrak{R}_{\text{crit}}} = \frac{4}{P_{\text{crit}}} \sqrt{\frac{3\pi\alpha^3\kappa_{\text{seed}}}{G\rho_{\text{frg}}(1+\kappa_{\text{seed}})}} = 0.345. \quad (32)$$

The size of the seed bodies under consideration is thus clearly not in conflict with the implied constraint. Even though this does not by itself determine what the actual

⁴ Note that by equating the left side of Equation (24) with zero (rather than making it larger than σ_{T}), one would readily obtain $P_{\text{rot}} = (48\pi\alpha^3/G)^{1/2} \rho_{\text{frg}}^{-1/2}$, which is a relevant condition for P_{rot} . To equate the constant with 3.3 hr, one would need $\alpha = 0.397$, the small difference from the value used being the product of the applied formalism.

⁵ Note that while the spin-period condition is independent of the body's size, the parallel introduction into the consideration of the constraint (27) makes it size-dependent.

Table 6
Tensile Strength and Fragmentation Parameters

Tensile strength, σ_{T} (Pa)	Separation velocity, v_{sep} (m s ⁻¹)	Radius of seed objects, $\mathfrak{R}_{\text{seed}}$ (m)	Number of fragmentation events, n_{frg}
1	0.025	67	11
5	0.056	149	14
10	0.080	210	16
20	0.113	297	17
40	0.159	420	19
63	0.200	527	20
100	0.252	665	21

size of the seeds is, the result (32) is encouraging in that Equation (27) with a reasonably low value of κ_{seed} , that is, with an approximately constant separation velocity, is a plausible condition that could be applied when incorporating the process of cascading fragmentation into the model.

The next issue concerns the magnitude of the tensile strength of the Kreutz sungrazers. I rely here on a few independent sources. Attree et al. (2018) estimated that a *minimum* tensile strength needed to support overhanging cliffs on the surface of comet 67P/Churyumov-Gerasimenko was extremely low, on the order of 1 Pa. Tensile strengths between 1 and 150 Pa were previously proposed from similar investigations by Groussin et al. (2015) and by Vincent et al. (2017). On the other hand, from his research of tidal splitting and rotational breakup Davidsson (2001) concluded that a strength of $\lesssim 100 \text{ Pa}$ was consistent with the data.

Table 6 presents the separation velocity and a possible radius of the seeds, computed conservatively as a function of the tensile strength. The entries tabulated near the bottom appear to be more realistic in terms of both v_{sep} and $\mathfrak{R}_{\text{seed}}$. The (nearly) constant separation velocity implies a gradual spin-up on account of a systematically decreasing size of the boulders with every fragmentation event. Also, because of the action of torques, the boulders must tumble, so that the direction of the separation velocity is subject to chaotic behavior from one fracture to the next. The number of breakup events, which each fragment of each seed undergoes before reaching the estimated 5-meter radius of the smallest SOHO Kreutz sungrazers, is tabulated as n_{frg} in the last column. I return to issues involving the seeds in the following sections.

An important implication is that the seeds needed for the formation of the stream of SOHO Kreutz comets, are not to be confused with the primary products of the parent sungrazer's tidal splitting at perihelion. The seeds — apparently highly-active, irregularly-shaped, subkilometer-sized fragments — represent only a minor fraction of the mass lost in this process. This conclusion is not surprising because it is supported very obviously by the observed return to perihelion of one or more of the parent's main surviving fragment(s), the Great March Comet of 1843 and possibly the Great Comet of 1668 as remains of the Great Comet of 1106 in the case of Population I. Likewise corroborating is an apparent consensus that the mass of the SOHO stream is orders of magnitude smaller than the mass of a large sungrazer (e.g., Sekanina 2003; Knight et al. 2010).

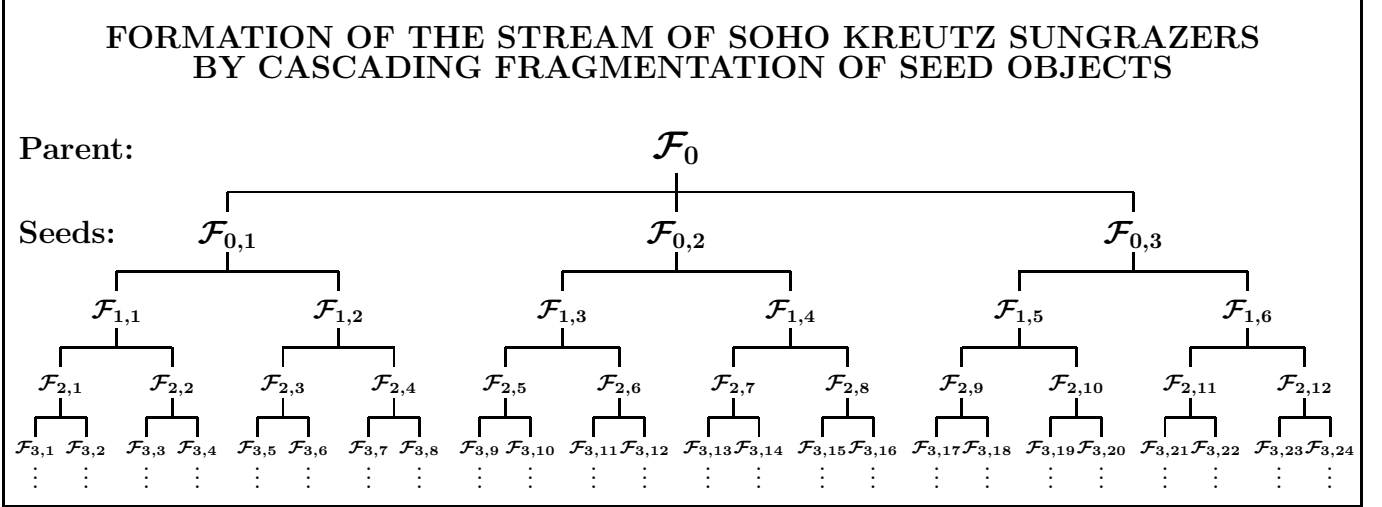


Figure 4. Schematic picture of the formation of the stream of SOHO Kreutz sungrazers by the process of cascading fragmentation of the seed objects, which effectively are fragments of generation zero. The depicted scenario shows the parent comet, \mathcal{F}_0 ; three seeds — $\mathcal{F}_{0,1}$, $\mathcal{F}_{0,2}$, and $\mathcal{F}_{0,3}$; six fragments of the first generation; 12 fragments of the second generation; and 24 fragments of the third generation.

4. FRAGMENTATION EVENTS' SPACING ALONG ORBIT

I argued in Section 3.2 that the seeds that give rise to the stream of SOHO sungrazers begin their existence at the time of tidal breakup of the parent comet. I designate the time of their birth as t_0 ; it may or may not coincide with the comet's perihelion time t_π , but the two times are never far apart. In line with the narrative of Section 3.2, the seeds are classified as fragments of generation zero; their number is n_{seed} ; they are referred to in the following by the symbols $\mathcal{F}_{0,1}, \mathcal{F}_{0,2}, \dots, \mathcal{F}_{0,n_{\text{seed}}}$; and their masses amount to $\mathcal{M}_{0,1}, \mathcal{M}_{0,2}, \dots, \mathcal{M}_{0,n_{\text{seed}}}$.

As stipulated in Section 3.2, the fragments of the first generation are born by a breakup of each seed into two halves, so that their total number equals $2n_{\text{seed}}$. A seed $\mathcal{F}_{0,k}$ fragments into $\mathcal{F}_{1,2k-1}$ and $\mathcal{F}_{1,2k}$, each then acquiring an extra momentum; if the seed's orbital velocity vector at the time is $\dot{\mathbf{r}}$ and its components in the RTN coordinate system⁶ $|\dot{\mathbf{r}}|_R$, $|\dot{\mathbf{r}}|_T$, and $|\dot{\mathbf{r}}|_N$, one fragment is released with an orbital velocity whose components are $|\dot{\mathbf{r}}|_R + v_R$, $|\dot{\mathbf{r}}|_T + v_T$, and $|\dot{\mathbf{r}}|_N + v_N$, the other with a velocity whose components are $|\dot{\mathbf{r}}|_R - v_R$, $|\dot{\mathbf{r}}|_T - v_T$, and $|\dot{\mathbf{r}}|_N - v_N$. Because the seed is expected to tumble, v_R , v_T , and v_N are modeled by means of a random number generator, yet they satisfy the condition $v_R^2 + v_T^2 + v_N^2 = v_{\text{sep}}^2$ (Section 3.3). The same rules apply to fragments of the higher generations, except that the number of fragments of a k -th generation is $2^k n_{\text{seed}}$ and its m -th fragment, $\mathcal{F}_{k,m}$, breaks up into fragments $\mathcal{F}_{k+1,2m-1}$ and $\mathcal{F}_{k+1,2m}$ of the $(k+1)$ -st generation (Figure 4).

The number and orbital positions of fragments depend strongly on the number of the seeds and on the locations in the orbit at which the seeds and fragments of the previous generations fractured. The spacing of the fragmentation events is thus another important factor that governs the structure of the SOHO sungrazers' stream.

⁶ The RTN right-handed orthogonal coordinate system is referred to the center and orbital plane of the body and rotates with it about the Sun. The R coordinate is in the direction away from the Sun, the N axis points to the north orbital pole, and the T coordinate is perpendicular to R in the plane.

I had previously addressed this issue (Sekanina 2002) in connection with the progressive fragmentation of the ill-fated comet D/1993 F2 (Shoemaker-Levy) before it impacted Jupiter in July 1994. The comet split tidally at the time of its close encounter with the planet in 1992 and continued to fragment nontidally along its final pre-impact joviocentric orbit. Investigation of this fragmentation sequence (Sekanina et al. 1998) showed that the rate of breakup episodes in the nontidal phase was subsiding with time, possibly a fundamental property of the process. If so, a similar slowdown should be expected for the Kreutz sungrazers. Accordingly, I subscribe to the fragmentation-chain law tested on comet Shoemaker-Levy and assume that a progression of breakup events started with the birth of the seeds at time t_0 and continued in a fashion, illustrated on a particular branch of fragments in the following:

Let a seed $\mathcal{F}_{0,k}$ split into the first-generation fragments $\mathcal{F}_{1,2k-1}$ and $\mathcal{F}_{1,2k}$ at time $t_1 = t_0 + \Delta t_0$. Next, let $m = 2k - 1$ or $m = 2k$ and $\mathcal{F}_{1,m}$ split into $\mathcal{F}_{2,2m-1}$ and $\mathcal{F}_{2,2m}$ at time $t_2 = t_1 + \Delta t_1$, where $\Delta t_1 = \Lambda \Delta t_0$ and the parameter $\Lambda > 1$ describes the slowdown rate. Similarly, let all fragments of the second generation split into fragments of the third generation at time $t_3 = t_2 + \Delta t_2$, where $\Delta t_2 = \Lambda \Delta t_1 = \Lambda^2 \Delta t_0$, etc. Generally, fragments of a k -th generation are produced by fragments of a $(k-1)$ -st generation at a time

$$t_k = t_{k-1} + \Lambda^{k-1} \Delta t_0. \quad (33)$$

The rate of increase in the lengths of intervals Δt_k follows a geometric progression, so that the fragmentation times t_k make up a sequence

$$t_k = t_0 + \frac{\Lambda^k - 1}{\Lambda - 1} \Delta t_0. \quad (34)$$

In the limit, using L'Hospital's rule,

$$\lim_{\Lambda \rightarrow 1} (t_k - t_0) = \lim_{\Lambda \rightarrow 1} (k \Lambda^{k-1} \Delta t_0) = k \Delta t_0, \quad (35)$$

as expected.

Equation (34) becomes an important boundary condition when written for the arrival time of a seed or a fragment to perihelion, $t_k = t_{\text{ref}}$. Then one can write $t_{\text{ref}} - t_0 = P_{\text{frg}}$, the orbital period, the exponent k in Equation (34) becoming the number of fragmentation events n_{frg} that the seed and its fragments undergo in order that an initial diameter $\mathfrak{R}_{\text{seed}}$ is reduced to a diameter $\mathfrak{R}_{\text{min}}$ of the smallest dwarf sungrazers detectable by the SOHO coronagraphs, adopted in Section 3.3 to amount to 10 meters; n_{frg} also equals the number of fragment generations. Listed in Table 6, it is derived from Equation (23) on the assumption that a fragment's mean dimension varies as a cube root of its mass,

$$n_{\text{frg}} = \frac{\log \mathcal{N}_0}{\log 2} \simeq 10 \log \left(\frac{\mathfrak{R}_{\text{seed}}}{\mathfrak{R}_{\text{min}}} \right), \quad (36)$$

where

$$\mathcal{N}_0 = \left(\frac{\mathfrak{R}_{\text{seed}}}{\mathfrak{R}_{\text{min}}} \right)^3 \quad (37)$$

is the total number of SOHO-like sungrazers collected from a seed. For example, for $\mathfrak{R}_{\text{seed}} \simeq 40$ to $100 \mathfrak{R}_{\text{min}}$ one finds $n_{\text{frg}} = 16$ to 20 and $\mathcal{N}_0 \simeq 6.5 \times 10^4$ to 10^6 .

With t_{ref} replacing t_k , Equation (34) reads

$$P_{\text{frg}} = \frac{\Lambda^{n_{\text{frg}}} - 1}{\Lambda - 1} \Delta t_0, \quad (38)$$

linking four parameters. But $P_{\text{frg}} \simeq 900$ yr for the sungrazer stream of Population I in the early 21-st century and the number of fragment generations n_{frg} cannot deviate much from 16 or 20, as the seeds cannot be much smaller or larger than adopted above. Equation (38) then becomes a relationship between Λ and Δt_0 . And for any such pair Equation (34) allows one to compute the fragmentation times for each of the n_{frg} generations of fragments, as exhibited in Table 7 (Δt_0 equaling by definition the interval of time between the births of the seed and the fragments of the first generation) with P_{frg} and n_{frg} held constant.

The reader should be aware of an ambiguity regarding the numbering of the fragmentation cycles, depending on their perception. In particular, the simulation process is terminated at the time of *birth* of the pair of fragments of the n_{frg} -th generation, which is the same as the time of *breakup* of their parent, a fragment of the $(n_{\text{frg}} - 1)$ -st generation.

Table 7 shows that an increase from 1.1 to 1.7 in the parameter Λ results in a drop by three orders of magnitude in the parameter Δt_0 . The higher the value of Λ , the more crowded the fragmentation events are in the early post-perihelion period of time. The major significance of this crowding for the eventual distribution of SOHO-like sungrazers is apparent from Section 5.

Table 7 also exhibits the increasing asymmetry between the numbers of pre- and post-aphelion fragmentation episodes as Λ increases. For $\Lambda = 1.1$ the first 14 events occur before aphelion, whereas for $\Lambda = 1.5$ to 1.7 the number increases to 18. The condition for the number of pre-aphelion fragmentation events, n_{pre} , is given by

$$n_{\text{pre}} = \text{trunc} \left\{ \frac{\log \left[1 + \frac{1}{2} (\Lambda - 1) P_{\text{frg}} / \Delta t_0 \right]}{\log \Lambda} \right\}. \quad (39)$$

Table 7

Sequence of Fragmentation Events Along Orbit ($P_{\text{frg}} = 900$ yr)
As Function of Slowdown Parameter Λ

Fragment generation	Time of fragmentation event (in yr from AD 1106) for slowdown parameter Λ				
	1.1	1.2	1.3	1.5	1.7
1	15.7	4.8	1.4	0.14	0.016
2	33.0	10.6	3.3	0.34	0.042
3	52.0	17.5	5.7	0.64	0.087
4	72.9	25.9	8.8	1.1	0.16
5	95.9	35.9	12.9	1.8	0.29
6	121.2	47.9	18.2	2.8	0.51
7	149.1	62.3	25.1	4.4	0.89
8	179.7	79.5	34.1	6.7	1.5
9	213.4	100.3	45.7	10.1	2.6
10	250.4	125.1	60.9	15.3	4.4
11	291.2	155.0	80.6	23.2	7.6
12	336.0	190.8	106.2	34.9	12.9
13	385.3	233.8	144.7	52.4	21.9
14	439.6	285.4	182.7	78.8	37.3
15	499.3	347.3	238.9	118.3	63.4
16	564.9	421.6	312.0	177.6	107.7
17	637.1	510.7	407.1	266.5	183.2
18	716.5	617.7	530.6	399.9	311.4
19	803.9	746.0	691.2	600.0	529.4
20	900.0	900.0	900.0	900.0	900.0

It is straightforward to set the condition for Λ to signal the absence of fragmentation events along the post-aphelion leg of the orbit. Writing Equation (38) for the pre-aphelion half of the orbit as

$$\frac{1}{2} P_{\text{frg}} \geq \frac{\Lambda^{n_{\text{pre}}} - 1}{\Lambda_{\text{pre}} - 1} \Delta t_0 \quad (40)$$

and dividing this expression by Equation (38), one finds a condition for Λ_{pre} :

$$\Lambda_{\text{pre}} \geq 2 - \Lambda_{\text{pre}}^{1 - n_{\text{frg}}}. \quad (41)$$

For large values of n_{frg} , which I consider in this paper, the post-aphelion half of the orbit is free from fragmentation events when Λ_{pre} is nearly exactly 2 or larger.

In Part I, I mentioned occasional observations of close pairs of SOHO sungrazers that provide evidence on relatively recent and definitely post-aphelion events of fragmentation. Such scenarios require values of Λ substantially lower than 2. In general, fragmentation histories of the seed objects clearly vary widely from case to case. One of the tasks of the proposed simulation computations is to examine a range of such variations.

5. ORBITAL PERTURBATIONS OF FRAGMENTS

In a breakup of a parent fragment, equal orbital momenta of opposite signs are assumed to be transferred to the two generated subfragments of equal mass, a basic scenario adopted here to incorporate the effects of cascading fragmentation into a model for the SOHO stream formation. The orbital-velocity vector for one of the new fragments is simulated by adding a separation velocity vector to the orbital-velocity vector of the parent fragment, while for the other new fragment its orbital-velocity vector is modeled by subtracting the same separation velocity vector from the parent's orbital-velocity

vector. The separation velocity vector is oriented at random, a product of the fragments' expected tumbling, whereas its magnitude is tentatively estimated at being close to 0.2 m s^{-1} (Table 6).

The components of the separation velocity affect the fragments' orbital elements, which differ, usually only slightly, from the orbital elements of the parent. In a sense, one can say that the products of a sequence of fragmentation events move in *perturbed* orbits. The degree of orbital similarity is measured by a *dispersion* in each orbital element, a method extensively used in Part I of this investigation to describe the observed structure of the stream of SOHO sungrazers. To understand the relationships among the dispersions of the orbital elements, it is desirable to examine the magnitudes of these separation velocity driven orbital *perturbations* as a function of not only the separation velocity vectors but the orbital positions of the parent at the fragmentation times as well. This examination requires the computation of the perturbed orbital motion of each simulated fragment, a topic that I am addressing next.

5.1. Computing Elements of a Fragment's Orbit

Let a Kreutz sungrazer move about the Sun unaffected by the planetary perturbations and let its orbit be determined by the argument of perihelion ω , the longitude of the ascending node Ω , the inclination i , the perihelion distance q , and the orbital period P . Let the comet pass through perihelion at time t_π^0 and break up at time t_{frg} , where $t_\pi^0 \leq t_{\text{frg}} < t_\pi$ and t_π is the time of return to perihelion, $t_\pi = t_\pi^0 + P$. Let the comet's heliocentric distance and true anomaly at t_{frg} be, respectively, $r(t_{\text{frg}}) = r_{\text{frg}}$ and $u(t_{\text{frg}}) = u_{\text{frg}}$. An outcome of the breakup event is the birth of a fragment that separates at a rate of v_{sep} relative to the main, parent mass.

An RTN right-handed orthogonal coordinate system, whose origin is in the parent's center of mass, the R axis pointing radially away from the Sun, the T axis in the orbital plane and perpendicular to R, and the N axis normal to this plane, has already been introduced in Section 4. Let the components of the fragment's separation velocity vector \mathbf{v}_{sep} in the cardinal directions of the RTN system be v_R , v_T , and v_N . This velocity vector prompts the fragment to end up in a new orbit, described by the asterisk-labeled elements

$$\begin{aligned}\omega^* &= \omega + \Delta\omega(t_{\text{frg}}, \mathbf{v}_{\text{sep}}), \\ \Omega^* &= \Omega + \Delta\Omega(t_{\text{frg}}, \mathbf{v}_{\text{sep}}), \\ i^* &= i + \Delta i(t_{\text{frg}}, \mathbf{v}_{\text{sep}}), \\ q^* &= q + \Delta q(t_{\text{frg}}, \mathbf{v}_{\text{sep}}), \\ P^* &= P + \Delta P(t_{\text{frg}}, \mathbf{v}_{\text{sep}}), \\ t_\pi^* &= t_\pi + \Delta t_\pi(t_{\text{frg}}, \mathbf{v}_{\text{sep}}).\end{aligned}\quad (42)$$

The aim of this exercise is to derive $\Delta\omega$, \dots , Δt_π as a function of the time, t_{frg} , of the fragmentation event (which determines the parent comet's orbital state vectors) and the fragment's separation velocity vector, \mathbf{v}_{sep} .

To begin, I assume that at the fragmentation time the parent comet's position vector and orbital-velocity vector in the ecliptic coordinate system equal \mathbf{S}_{frg} and \mathbf{V}_{frg} , respectively:

$$\mathbf{S}_{\text{frg}} = (x_{\text{frg}}, y_{\text{frg}}, z_{\text{frg}}), \quad \mathbf{V}_{\text{frg}} = (\dot{x}_{\text{frg}}, \dot{y}_{\text{frg}}, \dot{z}_{\text{frg}}). \quad (43)$$

They are given by the expressions:

$$\begin{pmatrix} x_{\text{frg}} \\ y_{\text{frg}} \\ z_{\text{frg}} \end{pmatrix} = r_{\text{frg}} \begin{pmatrix} P_x & Q_x \\ P_y & Q_y \\ P_z & Q_z \end{pmatrix} \times \begin{pmatrix} \cos u_{\text{frg}} \\ \sin u_{\text{frg}} \\ 0 \end{pmatrix}, \quad (44)$$

and

$$\begin{pmatrix} \dot{x}_{\text{frg}} \\ \dot{y}_{\text{frg}} \\ \dot{z}_{\text{frg}} \end{pmatrix} = \frac{k_0}{\sqrt{p}} \begin{pmatrix} P_x & Q_x \\ P_y & Q_y \\ P_z & Q_z \end{pmatrix} \times \begin{pmatrix} -\sin u_{\text{frg}} \\ e + \cos u_{\text{frg}} \\ 0 \end{pmatrix}, \quad (45)$$

where p is the orbit parameter in AU and k_0 the Gaussian gravitational constant in $\text{AU}^{\frac{3}{2}} \text{ day}^{-1}$. The directional cosines P_x, \dots, Q_z , are, together with R_x, R_y , and R_z (used below), the ecliptic components of the unit vectors \mathbf{P} , \mathbf{Q} , and \mathbf{R} in the orthogonal coordinate system tied to the orbital plane and the line of apsidal:

$$\begin{pmatrix} P_x & P_y & P_z \\ Q_x & Q_y & Q_z \\ R_x & R_y & R_z \end{pmatrix} = \begin{pmatrix} \cos \omega & \sin \omega & 0 \\ -\sin \omega & \cos \omega & 0 \\ 0 & 0 & 1 \end{pmatrix} \times \begin{pmatrix} 1 & 0 & 0 \\ 0 & \cos i & \sin i \\ 0 & -\sin i & \cos i \end{pmatrix} \times \begin{pmatrix} \cos \Omega & \sin \Omega & 0 \\ -\sin \Omega & \cos \Omega & 0 \\ 0 & 0 & 1 \end{pmatrix}. \quad (46)$$

At the fragmentation time, t_{frg} , the position vector of the fragment, $\mathbf{S}_{\text{frg}}^*$, is taken to coincide with the parent's position vector, while the fragment's orbital-velocity vector, $\mathbf{V}_{\text{frg}}^*$, is the sum of the parent's orbital-velocity vector and the fragment's separation velocity vector, \mathbf{v}_{sep} , whose ecliptic components are v_x , v_y , and v_z ,

$$\begin{pmatrix} x_{\text{frg}}^* \\ y_{\text{frg}}^* \\ z_{\text{frg}}^* \end{pmatrix} = \begin{pmatrix} x_{\text{frg}} \\ y_{\text{frg}} \\ z_{\text{frg}} \end{pmatrix}, \quad \begin{pmatrix} \dot{x}_{\text{frg}}^* \\ \dot{y}_{\text{frg}}^* \\ \dot{z}_{\text{frg}}^* \end{pmatrix} = \begin{pmatrix} \dot{x}_{\text{frg}} \\ \dot{y}_{\text{frg}} \\ \dot{z}_{\text{frg}} \end{pmatrix} + \begin{pmatrix} v_x \\ v_y \\ v_z \end{pmatrix}. \quad (47)$$

The ecliptic components of the separation velocity vector are related to its components in the RTN coordinate system by

$$\begin{pmatrix} v_x \\ v_y \\ v_z \end{pmatrix} = \begin{pmatrix} P_x & Q_x & R_x \\ P_y & Q_y & R_y \\ P_z & Q_z & R_z \end{pmatrix} \times \begin{pmatrix} \cos u_{\text{frg}} & -\sin u_{\text{frg}} & 0 \\ \sin u_{\text{frg}} & \cos u_{\text{frg}} & 0 \\ 0 & 0 & 1 \end{pmatrix} \times \begin{pmatrix} v_R \\ v_T \\ v_N \end{pmatrix}. \quad (48)$$

The determination of the fragment's orbital elements can now proceed by introducing the angular-momentum vector components:

$$\begin{aligned}\mathfrak{S}_{xy} &= \begin{vmatrix} x_{\text{frg}} & y_{\text{frg}} \\ \dot{x}_{\text{frg}}^* & \dot{y}_{\text{frg}}^* \end{vmatrix}, \\ \mathfrak{S}_{yz} &= \begin{vmatrix} y_{\text{frg}} & z_{\text{frg}} \\ \dot{y}_{\text{frg}}^* & \dot{z}_{\text{frg}}^* \end{vmatrix}, \\ \mathfrak{S}_{zx} &= \begin{vmatrix} z_{\text{frg}} & x_{\text{frg}} \\ \dot{z}_{\text{frg}}^* & \dot{x}_{\text{frg}}^* \end{vmatrix}.\end{aligned}\quad (49)$$

The following computations allow to incorporate, if deemed desirable, a nongravitational acceleration into the orbital motion of the fragment on the assumptions that it points in the antisolar direction and varies inversely as the square of heliocentric distance, the constraints employed by Hamid & Whipple (1953) in their investigation and likewise integrated into the standard

model for the split comets (Sekanina 1982). Let γ_0 be a dimensionless parameter describing the fragment's non-gravitational acceleration in units of 10^{-5} the Sun's gravitational acceleration. The fragment's *effective* Gaussian gravitational constant k_0^* , which replaces k_0 below, equals

$$k_0^* = \sqrt{k_0^2 - 10^{-5}\gamma_0 k_0^2} = k_0 \sqrt{1 - 10^{-5}\gamma_0}. \quad (50)$$

The fragment's longitude of the ascending node, Ω^* , inclination, i^* , and orbit parameter, p^* , related to the perihelion distance, q^* , via the orbital eccentricity, e^* , by $p^* = q^*(1+e^*)$, follow from the relations,

$$\begin{pmatrix} \widehat{\mathcal{S}}_{xy} \\ \widehat{\mathcal{S}}_{yz} \\ \widehat{\mathcal{S}}_{zx} \end{pmatrix} = k_0^* \sqrt{p^*} \begin{pmatrix} \cos i^* \\ \sin \Omega^* \sin i^* \\ -\cos \Omega^* \sin i^* \end{pmatrix}. \quad (51)$$

For the longitude of the ascending node one finds

$$\tan \Omega^* = -\frac{\widehat{\mathcal{S}}_{yz}}{\widehat{\mathcal{S}}_{zx}}, \quad \text{sign}(\sin \Omega^*) = \text{sign}(\widehat{\mathcal{S}}_{yz}); \quad (52)$$

for the inclination

$$\tan i^* = \frac{\sqrt{\widehat{\mathcal{S}}_{yz}^2 + \widehat{\mathcal{S}}_{zx}^2}}{\widehat{\mathcal{S}}_{xy}}, \quad (53)$$

where the sign of the denominator determines the quadrant of the inclination; and for the parameter

$$p^* = \frac{\widehat{\mathcal{S}}_{xy}^2 + \widehat{\mathcal{S}}_{yz}^2 + \widehat{\mathcal{S}}_{zx}^2}{(k_0^*)^2}. \quad (54)$$

Next, the fragment's orbital eccentricity is

$$e^* = \sqrt{1 + p^* \left\{ \frac{1}{(k_0^*)^2} \left[(\dot{x}_{\text{frg}}^*)^2 + (\dot{y}_{\text{frg}}^*)^2 + (\dot{z}_{\text{frg}}^*)^2 \right] - \frac{2}{r_{\text{frg}}} \right\}}, \quad (55)$$

so that the perihelion distance comes out from

$$q^* = \frac{p^*}{1+e^*} \quad (56)$$

and the orbital period from

$$P^* = \frac{2\pi}{k_0^*} \left(\frac{q^*}{1-e^*} \right)^{\frac{3}{2}}. \quad (57)$$

The fragment's true anomaly at the time of separation from the primary is given by

$$\sin u_{\text{frg}}^* = \frac{\sqrt{p^*}}{k_0^* e^* r_{\text{frg}}} (x_{\text{frg}} \dot{x}_{\text{frg}}^* + y_{\text{frg}} \dot{y}_{\text{frg}}^* + z_{\text{frg}} \dot{z}_{\text{frg}}^*) \quad (58)$$

with $\text{sign}(\cos u_{\text{frg}}^*) = \text{sign}(p^* - r_{\text{frg}})$. The sum of the argument of perihelion and the true anomaly at separation are calculated from

$$\cos(\omega^* + u_{\text{frg}}^*) = \frac{x_{\text{frg}} \cos \Omega^* + y_{\text{frg}} \sin \Omega^*}{r_{\text{frg}}} \quad (59)$$

with $\text{sign}[\sin(\omega^* + u_{\text{frg}}^*)] = \text{sign}(z_{\text{frg}})$. Equations (58) and (59) isolate the argument of perihelion. Finally, to derive the time of the fragment's return to perihelion, t_π^* , one

first gets the eccentric anomaly at separation, ϵ_{frg}^* ,

$$\epsilon_{\text{frg}}^* = 2 \arctan \left(\sqrt{\frac{1-e^*}{1+e^*}} \tan \frac{1}{2} u_{\text{frg}}^* \right), \quad (60)$$

which provides the following relation for the perihelion time:

$$t_\pi^* = t_{\text{frg}} - \frac{\epsilon_{\text{frg}}^* - e^* \sin \epsilon_{\text{frg}}^*}{k_0^*} \left(\frac{q^*}{1-e^*} \right)^{\frac{3}{2}}. \quad (61)$$

The eccentric anomaly ϵ_{frg}^* is here in radians and its range for fragmentation times t_{frg} between t_π^0 and t_π^* is $-2\pi \leq \epsilon_{\text{frg}}^* \leq 0$. Inserting ω^*, \dots, t_π^* into Equation (42) completes the derivation of effects of the orbital location of the fragmentation event and the separation velocity of the fragment on its orbital elements relative to those of the parent, $\Delta\omega(t_{\text{frg}}, \mathbf{v}_{\text{sep}}), \dots, \Delta t_\pi(t_{\text{frg}}, \mathbf{v}_{\text{sep}})$.

5.2. Perturbations of Fragment's Motion As Function of Location of Fragmentation Event in Orbit

Equations (52) to (61) provide a means to map out the structure of the stream of SOHO Kreutz sungrazers in general and examine their orbital-dispersion relationships in particular. Focusing on Population I again, I summarize in Table 8 the separation velocity driven perturbations of the key orbital elements of a fragment as a function of a breakup event's location in the orbit. The separation velocity in one of six cardinal directions is normalized to 1 m s^{-1} and the parent (which could be a seed or a fragment of lower generation) is assumed to move in the orbit of the Great March Comet of 1843, but with a period of 900 years, returning to perihelion in the year 2006. The orbit of the 1843 sungrazer is believed to provide an appropriate approximation to the orbit of X/1106 C1 at the time of interest.

I tabulate the perturbations of three elements of fragments' orbits that have been deemed especially important: (i) those of the longitude of the ascending node, triggered off by the normal component of the separation velocity; (ii) those of the perihelion distance, precipitated by the velocity's transverse component; and (iii) those of the time of return to perihelion, prompted by both the radial and transverse components.

I do not tabulate the perturbations of the orbit inclination, triggered off by the normal component and strongly correlated with the more prominent perturbations of the longitude of the ascending node; the perturbations of the argument of perihelion, due primarily to the normal component, but with a minor contribution from the transverse component as well; and the perturbations of the orbit eccentricity, due to the transverse and radial components, and correlated with the perturbations of the time of the fragment's return to perihelion via its orbital period.

The table documents the correlations between each of the three components of the separation velocity and the elements affected. Likewise, the extreme properties of a sungrazing orbit illustrate dramatically the dependence of a perturbation on the orbital location of the comet at the time of fragmentation. In particular, a breakup near perihelion may affect considerably the orbital period and thus the time of return to perihelion but practically has no effect on the longitude of the ascending node (and the

Table 8
 Perturbations of Selected Orbital Elements As Function of Orbital Location of Fragmentation Event
 (Orbit of Great March Comet of 1843, But With Orbital Period $P = 900$ yr; Equinox J2000)

At fragmentation time		Perturbation of orbital element/By separation velocity's							
Distance from Sun (AU)	Time to next perihelion (yr) ^a	ascending-node long.		perihelion distance (R_{\odot})		time of return to perihelion (days) ^b			
		normal component		transverse component		radial component		transverse component	
		+1 m s ⁻¹	-1 m s ⁻¹	+1 m s ⁻¹	-1 m s ⁻¹	+1 m s ⁻¹	-1 m s ⁻¹	+1 m s ⁻¹	-1 m s ⁻¹
$q = 0.00546$	900.000	0°000	0°000	0.000	0.000	0.00	0.00	+189.85 ^y	-140.49 ^y
0.006	$P - 0.011^d$	0.000	0.000	0.000	0.000	+48.35 ^y	-44.38 ^y	+170.13 ^y	-129.39 ^y
0.008	$P - 0.026^d$	0.000	0.000	0.000	0.000	+80.89 ^y	-70.36 ^y	+122.84 ^y	-100.08 ^y
0.01	$P - 0.039^d$	0.000	0.000	0.000	0.000	+86.97 ^y	-74.91 ^y	+96.12 ^y	-81.60 ^y
0.02	$P - 0.102^d$	0.000	0.000	0.000	0.000	+77.17 ^y	-67.52 ^y	+46.03 ^y	-42.41 ^y
0.05	$P - 0.352^d$	-0.001	+0.001	0.000	0.000	+52.90 ^y	-48.18 ^y	+17.95 ^y	-17.38 ^y
0.1	$P - 0.935^d$	-0.003	+0.003	0.000	0.000	+38.02 ^y	-35.52 ^y	+8.903 ^y	-8.758 ^y
0.2	899.993	-0.006	+0.006	0.000	0.000	+27.00 ^y	-25.71 ^y	+4.433 ^y	-4.397 ^y
0.5	899.973	-0.015	+0.015	0.000	0.000	+17.05 ^y	-16.53 ^y	+646.2	-644.0
1	899.924	-0.030	+0.030	+0.001	-0.001	+12.02 ^y	-11.76 ^y	+322.8	-322.2
2	899.786	-0.062	+0.062	+0.001	-0.001	+8.459 ^y	-8.328 ^y	+161.4	-161.1
3	899.607	-0.093	+0.093	+0.002	-0.002	+6.881 ^y	-6.794 ^y	+107.6	-107.4
5	899.153	-0.155	+0.155	+0.004	-0.004	+5.295 ^y	-5.244 ^y	+64.57	-64.44
7	898.593	-0.218	+0.218	+0.005	-0.005	+4.448 ^y	-4.411 ^y	+46.13	-46.02
10	897.586	-0.311	+0.312	+0.008	-0.008	+3.688 ^y	-3.663 ^y	+32.30	-32.19
15	895.529	-0.467	+0.468	+0.011	-0.011	+2.967 ^y	-2.950 ^y	+21.55	-21.44
20	893.057	-0.623	+0.625	+0.015	-0.015	+924.4	-920.0	+16.17	-16.06
25	890.211	-0.780	+0.782	+0.019	-0.019	+814.2	-810.8	+12.94	-12.83
30	887.016	-0.936	+0.939	+0.023	-0.023	+731.7	-728.9	+10.78	-10.68
40	879.630	-1.247	+1.254	+0.030	-0.030	+613.3	-611.3	+8.08	-7.98
50	870.962	-1.559	+1.569	+0.038	-0.037	+530.0	-528.4	+6.46	-6.35
60	861.020	-1.870	+1.884	+0.046	-0.045	+466.4	-465.2	+5.37	-5.26
80	837.163	-2.490	+2.515	+0.061	-0.060	+372.5	-371.7	+3.98	-3.88
100	807.419	-3.109	+3.148	+0.077	-0.074	+303.3	-302.7	+3.13	-3.03
120	770.445	-3.727	+3.781	+0.092	-0.089	+247.5	-247.1	+2.52	-2.43
140	723.569	-4.342	+4.414	+0.108	-0.103	+199.1	-198.8	+2.06	-1.97
160	659.722	-4.955	+5.048	+0.124	-0.118	+153.7	-153.5	+1.65	-1.57
180	555.779	-5.567	+5.683	+0.140	-0.132	+102.9	-102.8	+1.21	-1.14
186.429	450.000	-5.765	+5.887	+0.145	-0.137	+67.86	-67.81	+0.891	-0.839
180	344.221	-5.572	+5.684	+0.140	-0.132	+42.41	-42.38	+0.636	-0.600
160	240.278	-4.964	+5.051	+0.124	-0.118	+23.66	-23.64	+0.419	-0.398
140	176.431	-4.352	+4.418	+0.108	-0.103	+14.86	-14.85	+0.299	-0.286
120	129.555	-3.737	+3.785	+0.092	-0.089	+9.43	-9.43	+0.215	-0.207
100	92.581	-3.120	+3.153	+0.077	-0.074	+5.82	-5.82	+0.151	-0.146
80	62.837	-2.501	+2.521	+0.061	-0.060	+3.37	-3.37	+0.101	-0.098
60	38.980	-1.879	+1.890	+0.046	-0.045	+1.74	-1.74	+0.062	-0.061
50	29.038	-1.567	+1.575	+0.038	-0.037	+1.16	-1.16	+0.046	-0.045
40	20.370	-1.255	+1.260	+0.030	-0.030	+0.714	-0.714	+0.032	-0.031
30	12.984	-0.942	+0.945	+0.023	-0.023	+0.388	-0.388	+0.020	-0.020
25	9.789	-0.785	+0.787	+0.019	-0.019	+0.265	-0.265	+0.015	-0.015
20	6.943	-0.629	+0.630	+0.015	-0.015	+0.167	-0.167	+0.011	-0.011
15	4.471	-0.472	+0.473	+0.011	-0.011	+0.092	-0.092	+0.007	-0.007
10	2.414	-0.315	+0.315	+0.008	-0.008	+0.040	-0.040	+0.004	-0.004
7	1.407	-0.221	+0.221	+0.005	-0.005	+0.020	-0.020	+0.002	-0.002
5	0.847	-0.158	+0.158	+0.004	-0.004	+0.010	-0.010	+0.001	-0.001
3	0.393	-0.095	+0.095	+0.002	-0.002	+0.004	-0.004	+0.001	-0.001
2	0.214	-0.063	+0.063	+0.001	-0.001	+0.002	-0.002	0.000	0.000
1	0.076	-0.032	+0.032	+0.001	-0.001	0.000	0.000	0.000	0.000
0.5	0.027	-0.016	+0.016	0.000	0.000	0.000	0.000	0.000	0.000
0.2	0.007	-0.006	+0.006	0.000	0.000	0.000	0.000	0.000	0.000
0.1	0.935 ^d	-0.003	+0.003	0.000	0.000	0.000	0.000	0.000	0.000
0.05	0.352 ^d	-0.001	+0.001	0.000	0.000	0.000	0.000	0.000	0.000

Notes.

^a For the first six entries, when the comet is less than 1 day from perihelion, the time of return to perihelion is given as the difference orbital period P minus time elapsed from the just passed perihelion in days (d). The times for the last two entries are given in days.

^b Perturbations of the time of return to perihelion exceeding 1000 days in absolute value are expressed in years (y).

other angular elements) or the perihelion distance. However, the reader should be aware that this scenario of a major perturbation of the orbital period is fundamentally different from the effect addressed in Section 2.1 and the following, where fragments were assumed to move at the time of separation at *exactly* the same orbital velocities; the driver of very different future motions was a slight difference between the heliocentric distances of the centers of mass of the fragments at the instant of breakup and no separation velocity was involved. On the other hand, here I assume that fragments were at *exactly* the same heliocentric distance at the time of breakup and they ended up in diverse orbits on account of their separation velocities. As is plainly demonstrated, fragmentation effects on the perihelion time could in either scenario be enormous.

In contrast to near-perihelion breakups, fragmentation near aphelion — and generally at large heliocentric distance — has only a very minor effect on the orbital period and on the time of a fragment’s return to perihelion. On the other hand, the events of disruption at these locations may greatly affect a fragment’s perihelion distance and/or the angular elements, the longitude of the ascending node in particular.

Interesting aspects of the perturbation variations are symmetries, of which there are two kinds. One of them, forward vs backward, is seen in Table 8 to be universal — columns 3 and 4 for the longitude of the ascending node; columns 5 and 6 for the perihelion distance; etc. — but always only approximate. The other symmetry, pre-aphelion vs post-aphelion, does not apply, obviously, to the time of return to perihelion. It applies approximately to the longitude of the ascending node, but for the perihelion distance the match is apparently perfect to better than $10^{-4} R_{\odot}$.

From Table 8 one can estimate a crude upper limit for the range of each element inherent to the stream of Kreutz sungrazers, which is consistent with the fragmentation parameters considered in Section 3.3, namely, a separation velocity of $\sim 0.2 \text{ m s}^{-1}$ per event and ~ 20 generations of fragments, equivalent to $\sim 4 \text{ m s}^{-1}$. One finds $\sim 20^+$ in the nodal longitude, 0.5 to 0.6 R_{\odot} in the perihelion distance, and nearly 1000 years in the perihelion time, on top of the adopted 900 yr orbital period. These numbers do by no means look excessive, given that the realistic ranges should amount to only a small fraction of the upper limits. They also suggest that the orbits of the seeds may be exhibiting a fairly wide range of periods that the subsequent process of cascading fragmentation is merely extending ever further.

5.3. Dispersions of SOHO Sungrazer Swarms As Fragments’ Orbital Perturbations

A striking result in Part I was the contradiction between the correlations of $\text{disp}(\Omega)$ with $\text{disp}(\hat{t}_{\pi})$ among the swarms of the SOHO Kreutz sungrazers in narrow intervals of the nodal longitude on the one hand and in time on the other hand. The two dispersions correlated inversely among the swarms of the first kind, when they ranged from $0^{\circ}.01$ to $0^{\circ}.1$ in the nodal longitude and from 2 to 7 years in the perihelion time. The dispersions varied in the same direction among the swarms of the second kind, when they averaged about 2° in the nodal longitude and about 1.3 days in the perihelion time.

Inspection of Table 8 shows that the *swarms in the nodal longitude*, which include sungrazers with nearly coinciding nodal longitudes, that is, with near-zero perturbations of this element, refer to objects sharing the early fragmentation history, mostly the first days and weeks after the seeds had separated from the parent comet. The table shows that in this period of time the perturbations of the nodal longitude and the perturbations of the perihelion time do vary in opposite directions. The magnitudes of the dispersions in time are also of the correct order of magnitude. For example, about 20 weeks after perihelion, when the tabulated perturbation of the nodal longitude is $0^{\circ}.093$, the perturbation of the perihelion time is about 6.8 years, or ~ 2500 days; for comparable nodal-longitude dispersions the first entries of Table 3 in Part I yield the perihelion-time dispersions near 2000 days, which actually is better agreement than one would expect.

For the SOHO sungrazers returning to perihelion nearly simultaneously (within, say, a few days of one another), which I referred to in Part I as the *swarms in time*, and whose dispersion in the nodal longitude equaled on the average a few degrees, expectation from Table 8 is that these objects share a history of breakups some tens of years before perihelion, when they are tens of AU from the Sun. The table suggests that at 1 m s^{-1} the perturbations of the nodal longitude and perihelion time both decline with progressing time of fragmentation. For example, a tabulated perturbation of the nodal line, equaling $\sim 2^{\circ}$ and implying a perturbation of ~ 2 days in the arrival time, could be achieved by a fragmentation event some 40 years before perihelion. At the same separation velocity, the perturbations are only 1° and 0.5 day, respectively, with an event about 25 years later.

The seemingly bizarre relationships between the dispersions in the SOHO sungrazers’ nodal longitudes and arrival times detected in Part I of this investigations are thus readily explained as orbital perturbations of the fragments’ motions exerted by the separation velocities acquired at breakup of their parent bodies, the fragments of the preceding generation.

The SOHO sungrazers are not the only Kreutz fragments that fit the presented perturbation scheme. The four nuclear fragments of the Great September Comet of 1882, for which Kreutz (1891) computed separate sets of orbital elements, appear to comply with the scheme as well, regardless of the nature of the mechanism that fragmented the comet’s parent nucleus. Using Kreutz’s results I derive in Table 9 the differences, in the longitude of the ascending node, in the perihelion distance, and in the time of return to perihelion (coinciding with the future orbital period taken from Table 1), between the individual nuclei and compute the dispersions $\text{disp}(\Omega)$, $\text{disp}(\hat{q})$, and $\text{disp}(\hat{t}_{\pi})$. Unfortunately, the dispersions in the nodal longitude and in the perihelion distance are so small that the mean errors (converted from Kreutz’s probable errors) exceed their values. Fair expectation is that the dispersion in the nodal longitude is less than $0^{\circ}.01$ and the dispersion in the perihelion distance less than $0.001 R_{\odot}$. From Table 8 both conditions give very soft limits on the fragmentation time, which nonetheless are consistent with the result from the dispersion in time — expectation that the fragmentation event took place within 30 minutes of perihelion.

Table 9
Orbital Differences and Dispersions for Nuclei A Through D
of Great September Comet of 1882

Nuclear fragments	Longitude of ascending node	Perihelion distance (R_{\odot})	Orbital period (yr)
A–B	$+0^{\circ}0003 \pm 0^{\circ}0064$	-0.00003 ± 0.00046	-84 ± 7
A–C	$+0.0018 \pm 0.0070$	-0.00011 ± 0.00049	-169 ± 8
A–D	$+0.0054 \pm 0.0076$	$+0.00024 \pm 0.00054$	-232 ± 11
B–C	$+0.0015 \pm 0.0048$	-0.00007 ± 0.00033	-85 ± 5
B–D	$+0.0051 \pm 0.0057$	$+0.00027 \pm 0.00040$	-148 ± 9
C–D	$+0.0036 \pm 0.0063$	$+0.00034 \pm 0.00044$	-63 ± 10
disp	$0^{\circ}0035 \pm 0^{\circ}0064$	0.00021 ± 0.00045	143 ± 9

6. MONTE CARLO SIMULATION OF THE SOHO STREAM: PUTTING THINGS TOGETHER

If the Kreutz system consists of nine discrete populations (Sekanina 2022b), it makes sense to perceive the observed stream of SOHO sungrazers as a sum of nine independent streams. It is hoped that a Monte Carlo simulation of the stream of Population I — by far the most prominent one — will be beneficial, at least to a point, to our understanding of the fundamental features of the other ones as well, even though significant variations in the arrival rates with time were revealed in Part I to exist among them.

6.1. The Objectives and the Algorithm

A major objective of this project is to fit the observed annual-rate curve of perihelion arrival for the stream of SOHO Population I sungrazers as closely as possible. The peak in 2006, seen in the histogram in the upper part of Figure 5 of Part I, is considered a fluke, which does not need to be computer simulated. On the other hand, the steady increase in the rate, supported by the data over the period of ten years, is deemed genetically significant. The total number of the Population I sungrazers in the stream, detected in the C2 coronagraph, is estimated to vary from about 60 per year in 2000 to 100 per year in 2009, with the rate of increase gradually diminishing with time, as indicated in Part I. The annual arrival rate of Population I sungrazers, \mathcal{N} , observed in C2 is approximately expressed by

$$\mathcal{N}(Y) = 60 + 5.1(Y - 2000) - 0.12(Y - 2000)^2, \quad (62)$$

where Y is the year (taken as an integer). Since as much as a half of the sungrazer population avoids the field of the C2 coronagraph because of seasonal effects, the absolute term on the right-hand side of Equation (62) may in fact be up to a factor of two higher. However, there is no evidence that the year-to-year trend should be affected. Although the Marsden orbits are unavailable after mid-2010, it appears that the annual arrival rate of Kreutz sungrazers stabilized more recently (Battams & Knight 2017) and I accept that this conclusion applies to Population I as well.

Another objective is to simulate the range of dispersion in the orbital elements as the number of fragment generations increases with time. In line with the results of Part I, I focus on three orbital elements: the perihelion times of the returning fragments, their longitudes of the ascending node, as well as their perihelion distances.

The reader will note that the model offers the user a breathtaking variety of options and a virtually endless range of choices in his effort to fit the stream’s observed structure. In the rest of this paper I examine an array of plausible scenarios and constraints on their parameters, search for an optimum solution to the annual arrival rate of the SOHO sungrazer stream, discuss the problem of dispersion in the orbital elements, and contemplate potential avenues for further work in the future.

The algorithm of the computer code follows closely the narrative in the preceding sections. The code allows the process to begin with a *single* seed, presumably a subkilometer-sized fragment of X/1106 C1, which is assumed, as one of countless products of the tidal fragmentation event at perihelion, to have separated from the parent on 1106 February 1.0 TT. This is a plausible date, whose uncertainty of a few days has no effect on the outcome.

To simplify the computations, the indirect planetary perturbations (the only ones of any impact on the problem) have been ignored, the orbits of the seed and its fragments taken as ideal ellipses. Given this constraint, an appropriate set of orbital elements (other than the starting perihelion time and orbital period) to use for the seed is that of the Great March Comet of 1843. And since the seed most obviously responsible for the stream of Population I sungrazers observed by SOHO is that in an orbit that would bring it back to perihelion at about this time, the appropriate orbital-period choice is approximately 900 years. This completes the problem of the seed’s initial orbit in the algorithm.

The pyramidal construct, illustrated schematically in Figure 4, has at this point been introduced with any one of the three marked $\mathcal{F}_{0,1}, \dots, \mathcal{F}_{0,3}$ at the top. The process of nontidal, cascading fragmentation has thus been set in motion, the seed breaking up rotationally into two equal halves, as described in Section 3.3. Each half has subsequently broken again into two equal halves, etc., until the fragments have reached average dimensions of the faint SOHO sungrazers, their size distribution ignored. There is nothing that could prevent the user to run the code as many times as he wishes, to complete the computations for n_{seed} different seeds, and to combine the outcomes into a single output.

On certain assumptions, a typical separation velocity acquired by fragments at breakup has, in terms of the tensile strength, been estimated at 0.2 m s^{-1} , but this may require much adjustment. A postulate of fragments tumbling out of control calls for use of a random-number generator to determine the separation velocity components in the radial, transverse, and normal directions of an orthogonal coordinate system (Sections 4 and 6.5). The formalism of breaking up into two halves of equal mass has required no additional assumptions to describe the fragments’ motions in the breakup’s aftermath, as the separation velocities gained by the pair should be of the same magnitude in opposite directions. When summed up with the parent’s orbital-velocity vector, the opposite separation velocity vectors make the two fragments end up in new orbits, thus contributing to the stream’s increased orbital scatter. The elements of these orbits depend not only on the separation velocity vectors, but substantially also on the location of the fragmentation episode in the orbit (Section 5 and Table 8).

The topic of orbital locations at which generations of fragments have been breaking up parallels the issue of separation velocity in the overall problem of cascading fragmentation. The history of the law proposed to describe a sequence of fragmentation events along the orbit has briefly been described in Section 4. I discuss the issue of incorporating the law into the model in greater detail in Section 6.3. Here I only note that its parameter, Λ , could be allowed to become a random quantity in an interval of up to, say, $1 < \Lambda < 2$, which excludes scenarios with fragmentation events limited to pre-aphelion locations (Section 4). Two additional parameters of the law have been kept constant (Section 6.3), so that the incorporation of the fragmentation process into the computer code exhibits a blending of features of random nature with deterministic ones. The process extends over a number of generations of fragments, as discussed in Section 4.

The outcome is a computer-simulated stream of members of Population I. In order to be ready for direct comparison with the observed stream of relevant SOHO sungrazers, the computer-generated list still has to be sorted by the quantity of interest (e.g., the perihelion arrival time), using a sorting code, and then prepared for graphics either as a cumulative distribution or in the form of a histogram. In an effort to fit genetically significant features of the observed stream, the entire procedure of computer simulation has to be iterated by trial and error to optimize the resulting solution.

6.2. Incorporation of the Seeds

The optimization is a complex process that involves every part of the algorithm. Of major importance are the dimensions and number of seeds as well as their locations in the chain of debris from the tidal fragmentation event at perihelion, all of which greatly affects the makeup and properties of the simulated stream of SOHO-like sungrazers.

Seed dimensions are the only of the three parameters that is subject to obvious constraints. The observed behavior of the SOHO sungrazers offers an estimate for the minimum size of a seed to survive the hostile environment. Even the brightest SOHO sungrazers undetectable from the ground, such as the pair of C/1998 K10 and K11, C/2003 K7, C/2008 K4, C/2010 G4, and others, whose peak brightness was near magnitude 0 (Knight et al. 2010, Sekanina & Kracht 2013), were not massive enough, disintegrating several hours before perihelion. And all sungrazers discovered with the coronagraphs on board the Solwind satellite (Michels et al. 1982, Sheeley et al. 1982) and Solar Maximum Mission (MacQueen & St. Cyr 1991), most of them in the same brightness category, met the same fate.

On the other hand, the sungrazer C/2011 W3, already mentioned in Section 2.4, had a peak brightness not fainter than magnitude -3 (Green 2011; estimates by two independent observers), survived perihelion but its nucleus perished less than 2 days after perihelion (Sekanina & Chodas 2012). The effective nuclear diameter at times well before the demise has by independent techniques been estimated at about 400 meters (Sekanina & Chodas 2012, McCauley et al. 2013, Raymond et al. 2018). The object was not a member of Population I, but it does not make much difference, because this was not the only

case of its kind observed. The “headless wonder” — a long dust tail emanating out of nothing — observed as a sungrazing comet C/1887 B1, which did happen to be a member of Population I, was another example of the same phenomenon (Section 2.4).

One cannot rule out that the event experienced by Lovejoy is of the kind that a seed needs to undergo to initiate the process of formation of its own stream. The dimensions of the largest debris left at the location of the former nucleus are unknown but some sizable boulders are always likely to survive intact or nearly intact; likewise, one certainly cannot exclude the possibility that the above description refers not to a single event but to a *sequence* of episodes, whose combined effect could from a distance of the terrestrial observer appear — and be interpreted — in a simplified manner.

Now, as described by Sekanina & Chodas (2012), a peculiar trait of the Lovejoy post-perihelion event was that, contrary to a typical comet disintegration episode, *no major flare-up* was observed, only a few relatively minor outbursts, the timing of the last one just about coinciding with the disintegration event, as determined from the variations in the spine-tail orientation. Also highly unusual (if not unique) was the sudden, dramatic, day-to-day transformation of the comet’s appearance (on December 19–20) and low dust velocities in the spine tail, estimated at 20–30 m s⁻¹. These observations prompted the authors to remark that, contemplated in its entirety, the event was reminiscent of a collapse of the nucleus rather than its explosion. One has a good reason to believe that — its seemingly healthy appearance notwithstanding — the comet was leaving perihelion already severely damaged and the 40-or-so hours were needed to complete the dismantling of the sick nucleus.

If these ideas are correct, one may have to admit that there could be two classes of seeds that generate streams of SOHO-like sungrazers: besides those released at perihelion from a massive sungrazer in the course of its nuclear splitting by tidal forces (such as the Great September Comet of 1882), there may exist solitary seeds (such as Lovejoy). In either case, the seeds appear to be recruited only from objects of a particular makeup and dimensions. A seed should be sizable and resilient enough to survive the perihelion environment, but small and weak enough to get its fabric damaged enough in the process to subsequently become prey to the forces of cascading fragmentation.

If one accepts that an average faint SOHO sungrazer is approximately $\mathfrak{R}_{\min} = 10$ meters across, then the inference that a seed should be about the size of the nucleus of comet Lovejoy would imply some 60,000 to 70,000 fragments per seed, if no major fraction of mass has been lost to microscopic dust. With the adopted formalism, a convenient analytical tool to approximate the actual process, these numbers would seem to call for 16 generations of fragments, as seen directly from Equation (36) or equivalently from

$$\mathfrak{R}_{\text{seed}} = \mathfrak{R}_{\min} 2^{\frac{1}{3}n_{\text{frg}}} = \mathfrak{R}_{\min} \exp(0.231 n_{\text{frg}}). \quad (63)$$

Because the stream of SOHO sungrazers demonstrates the existence of major scatter in both the arrival time and other elements, it is obvious that seeds fragment gradually, throughout the orbit.

6.3. Incorporation of the Orbital Distribution Law of Fragmentation Events

Direct use of Equation (33) in the Monte Carlo simulation code would be inconvenient because two random numbers would have to be assigned, one to Λ and a second to Δt_0 , whose value ought to be confined to some prescribed range. It is preferable to employ instead Equation (34) and relate the time scale to the fragmentation number, n_{frg} , via Λ , as in Equation (38).

In practice, the reference time t_{ref} in Equation (34) — following the text at the top of page 12 — is kept fixed, corresponding generally to a time by when the continuing process of cascading fragmentation reduces the dimensions of simulated fragments *below* the estimated sizes of the SOHO sungrazers. The time scale over which cascading fragmentation has been going on is about 900 years, unless the observed stream of SOHO Population I sungrazers is a product of a solitary Lovejoy-like Population I fragment that had separated from the parent comet to X/1106 C1 in AD 363 and barely survived the following perihelion passage. I deem this scenario too speculative to consider seriously and prefer to stay with X/1106 C1 as the source of Population I seeds.

As $\Delta t_0 = t_1 - t_0$, Equation (34) can be written thus:

$$t_1 = t_0 + \frac{\Lambda - 1}{\Lambda^{n_{\text{frg}} - 1}} (t_{\text{ref}} - t_0). \quad (64)$$

This is an expression for the period of time elapsed between the breakups of a seed and a first-generation fragment, $t_1 - t_0$, as a function of the parameter Λ , the fragmentation number, n_{frg} , and the reference time, t_{ref} . If in Equation (34) for t_{ref} I next insert the identities, $(t_2 - t_1)/\Lambda$ for Δt_0 , and $[(\Lambda + 1)t_1 - t_2]/\Lambda$ for t_0 , I obtain

$$t_2 = t_1 + \frac{\Lambda - 1}{\Lambda^{n_{\text{frg}} - 1} - 1} (t_{\text{ref}} - t_1), \quad (65)$$

an expression for the period of time elapsed between the breakups of a fragment of the first generation and a fragment of the second generation. Generally, the time between the breakups of a fragment of a k -th generation and a fragment of a $(k+1)$ -st generation is given by

$$t_{k+1} = t_k + \frac{\Lambda - 1}{\Lambda^{n_{\text{frg}} - k} - 1} (t_{\text{ref}} - t_k). \quad (66)$$

This formalism can conveniently be incorporated into the Monte Carlo simulation code, because it warrants that $t_{k+1} > t_k$ for any $k < n_{\text{frg}}$ and any $t_k < t_{\text{ref}}$.

Table 10
Times of Last SOHO Imaging of Bright Kreutz Sungrazers Before Their Disintegration

SOHO Kreutz sungrazer	Time of last imaging ^a (day)	Orbit MPC	Peak on magnitude	reference
C/2008 K4	-0.096	63377	0.5	Sekanina & Kracht (2013)
C/2010 G4	-0.118	72133	0	Sekanina & Kracht (2013)
C/1998 K10	-0.12	33650	0.8	Knight et al. (2010)
C/1998 K11	-0.14	33650	0.5	Knight et al. (2010)
C/2000 H2	-0.19	40669	0.7	Sekanina & Kracht (2013)

Note.

^a Reckoned from the time of perihelion passage.

Table 11
Maximum Allowed Fragmentation Numbers n_{frg} As Function of Parameter Λ

Λ	n_{frg}	Λ	n_{frg}	Λ	n_{frg}	Λ	n_{frg}
1.1	133	1.6	30	2.1	20	2.6	16
1.2	73	1.7	27	2.2	19	2.7	15
1.3	53	1.8	25	2.3	18	2.8	15
1.4	42	1.9	23	2.4	17	2.9	14
1.5	35	2.0	21	2.5	16	3.0	14

There are however two caveats. The first one is obvious: Equation (66) is not defined for $k = n_{\text{frg}}$, whereby the meaningless simultaneous arrival of all fragments to perihelion (Table 7) is automatically eliminated.

The second caveat concerns environmental limits on the time of the seed's *initial fragmentation event*, t_1 . This event must not take place too close to the Sun too soon after the seed's birth, in order to avoid the complete sublimation of the fragments of the first generation before the process of cascading fragmentation takes over. Denoting

$$\nu = \frac{t_{\text{ref}} - t_0}{t_1 - t_0}, \quad (67)$$

the condition requires that the time interval between the two breakup events, $t_1 - t_0$, exceed a particular minimum, thereby implying a maximum value of ν_{max} . A conservative estimate for $(t_1 - t_0)_{\text{min}}$ is obtained from the last SOHO observations of the brightest Kreutz sungrazers, of peak magnitudes between 0 and +1, before they disintegrated. The five with the known orbits, which the SOHO's C2 coronagraph was imaging down to the smallest heliocentric distances, are listed in Table 10. The suggested limit of $(t_1 - t_0)_{\text{min}} \simeq 0.1$ day, equivalent to a distance of a little over $4R_{\odot}$ from the Sun, together with $t_{\text{ref}} - t_0 \simeq 900$ yr, implies $\nu_{\text{max}} \simeq 3.3 \times 10^6$. From Equation (64) one gets the constraint on n_{frg} as follows:

$$n_{\text{frg}} < \frac{\log [1 + (\Lambda - 1)\nu_{\text{max}}]}{\log \Lambda}. \quad (68)$$

The highest allowed values of n_{frg} as a function of Λ are listed in Table 11. In a limit, L'Hospital's rule gives

$$\lim_{\Lambda \rightarrow 1} n_{\text{frg}} < \lim_{\Lambda \rightarrow 1} \frac{\Lambda \nu_{\text{max}}}{1 + (\Lambda - 1)\nu_{\text{max}}} = \nu_{\text{max}}. \quad (69)$$

The way the computer code was written, the standard output is a set of lists, sorted sequentially by three orbital elements, and histograms of all simulated fragments of a fixed n_{gen} -th generation, where $n_{\text{gen}} < n_{\text{frg}}$. It is now n_{gen} that controls the size ratio of the simulated SOHO sungrazers and seeds, as well as the total number of test fragments: rising n_{gen} by one increases the ratio of $\mathcal{R}_{\text{seed}}/\mathcal{R}_{\text{min}}$ by a factor of 1.26 and \mathcal{N} by a factor of two.

The model's simulation computations began on the assumption that $n_{\text{gen}} = 16$ and $n_{\text{frg}} = 20$, which required that Λ not exceed 2.13 according to Equation (68). To explain the existence of close pairs of SOHO sungrazers implying post-aphelion fragmentation, one should allow a limited number of fragments of generations between n_{gen} and n_{frg} or, alternatively, subjected to $\Lambda < 1.3$, if Λ is a random quantity (within limits).

6.4. Constants and Options

One of the tasks of this investigation is to find out how is the difference between n_{gen} and n_{frag} going to affect the simulated stream of sungrazers. This procedure could further be manipulated by changing the reference time t_{ref} , tied to the seed's orbit. This shows that the two free constants, n_{frag} and t_{ref} , have a significant impact on the outcome of the simulation.

The other constant that affects the simulated orbital evolution of fragments is their separation velocity. Nominally, its "recommended" magnitude, based on the considerations in Section 3.3, is 0.2 m s^{-1} , independent of fragment size and therefore implying spin-up. Since the overall dispersion of the orbital elements clearly correlates with the magnitude of the separation velocity, comparison of the simulated orbital sets with the observations should provide a valuable test of the constants.

The last topic that involves decisions of the optional nature is the problem of whether or not to incorporate a nongravitational acceleration in the orbital computations. While these effects on the motions of the SOHO Kreutz sungrazers in the final hours of their life is enormous (Sekanina & Kracht 2015b), I believe that — given other uncertainties — their overall contribution is not significant enough for inclusion.

6.5. Random Number Generator and Applications

A random-number generator routine supplies 10-digit random numbers \mathcal{R} in the range $0 < \mathcal{R} < 1$, working with several positive integers. Three of them are constants: A_0 and B_0 are on the order of 10^{13} to 10^{14} , while Z_0 is an odd number on the order of 10^2 . Two additional integers, \mathcal{A} and \mathcal{B} , are variable.

To begin the generation of random numbers, I choose \mathcal{A} such that it satisfies a condition

$$\mathcal{B} = \mathcal{A}Z_0 + A_0 \gg B_0 \quad (70)$$

and then compute

$$\mathcal{A}^* = \mathcal{B} \bmod B_0. \quad (71)$$

The first random number \mathcal{R} is given by

$$\mathcal{R} = \mathcal{A}^*/B_0. \quad (72)$$

Inserting \mathcal{A}^* for \mathcal{A} into Equation (70) and executing successively Equations (70) through (72), I get a second random number \mathcal{R} , etc.

Table 12
Runs to Test a Random Number Generator

Interval of random numbers	Percentage per interval in a set totaling			
	10^3	10^4	10^5	10^6
0.0 – 0.1	9.3	10.3	10.2	10.0
0.1 – 0.2	10.9	10.1	10.0	10.0
0.2 – 0.3	8.8	9.7	10.1	10.0
0.3 – 0.4	9.7	10.3	10.0	10.0
0.4 – 0.5	10.0	10.1	9.9	10.0
0.5 – 0.6	10.3	9.9	10.0	10.0
0.6 – 0.7	10.3	9.9	10.1	10.1
0.7 – 0.8	9.9	10.1	10.0	10.0
0.8 – 0.9	10.0	9.6	9.9	9.9
0.9 – 1.0	10.8	10.0	9.8	10.0

Next I have generated sets of random numbers, totaling a thousand, ten thousand, hundred thousand, and a million entries, respectively. Each set has been divided into ten equal intervals between 0 and 1, and a percentage of the total in each interval computed to test the degree of randomness. The results in Table 12 show, as expected, that the relative variations in the number of entries per interval drop with increasing size of the set.

Four random numbers are used in the computer simulations per fragmentation event: one for the parameter Λ and three for the separation velocity components. To complete the computations down to fragments of an n_{gen} -th generation requires a file of $4 \cdot (2^{n_{\text{gen}}} - 1)$ random numbers. A preferred range for Λ , $\Lambda_{\text{min}} < \Lambda < \Lambda_{\text{max}}$, where $\Lambda_{\text{min}} \geq 1$ and $\Lambda_{\text{max}} \leq 2$, is readily satisfied by

$$\Lambda = \Lambda_{\text{min}} + (\Lambda_{\text{max}} - \Lambda_{\text{min}}) \mathcal{R}. \quad (73)$$

When $\Lambda_{\text{min}} = \Lambda_{\text{max}}$, Λ becomes a parametric constant.

The separation velocity imposes a different condition on random numbers. The radial, transverse, and normal components should each be allowed to vary in extreme cases from $-v_{\text{sep}}$ to $+v_{\text{sep}}$, so that a component equaling zero is given by a random number of $\frac{1}{2}$. One can write

$$\begin{aligned} v_{\text{R}} &= v_{\text{sep}} \left(\mathcal{R}_1 - \frac{1}{2} \right) \lambda, \\ v_{\text{T}} &= v_{\text{sep}} \left(\mathcal{R}_2 - \frac{1}{2} \right) \lambda, \\ v_{\text{N}} &= v_{\text{sep}} \left(\mathcal{R}_3 - \frac{1}{2} \right) \lambda, \end{aligned} \quad (74)$$

where λ is a normalization constant. The condition that the sum of squares of the components equal the square of the separation velocity is equivalent to a condition

$$\lambda^2 \left[\left(\mathcal{R}_1 - \frac{1}{2} \right)^2 + \left(\mathcal{R}_2 - \frac{1}{2} \right)^2 + \left(\mathcal{R}_3 - \frac{1}{2} \right)^2 \right] = 1, \quad (75)$$

from which

$$\lambda = \frac{2}{\sqrt{3 - 4 \sum_{k=1}^3 \mathcal{R}_k (1 - \mathcal{R}_k)}}. \quad (76)$$

The normalization constant attains values of $\lambda > \frac{2}{3} \sqrt{3}$.

7. RESULTS FOR FRAGMENTS OF 16TH GENERATION

The results of Monte Carlo computations reported below present simulations of a semi-stochastic process that was to generate a stream of the SOHO Kreutz sungrazers of Population I as products of cascading fragmentation of a single seed, a subkilometer-sized object, born in the course of tidal fragmentation at perihelion. The seed was moving essentially in the orbit of the Great Comet of 1106, the seed's parent, but with an orbital period of ~ 900 yr, by ~ 163 years longer than the orbital period of C/1843 D1, the 1106 comet's principal fragment. Deemed appropriate as an approximation to the 1106 comet's orbit at the beginning of the 21st century (Section 6.1), an orbital solution for the 1843 comet derived by Sekanina & Chodas (2008) was adopted. The 1106 comet was assumed to have passed its perihelion on February 1.0 TT, the date from which time was reckoned.

In reality, the Population I stream is a sum of fragmentation products of a number of seeds from the 1106 parent comet that may or may not partially or completely overlap one another in time. In addition, the observed SOHO stream also contains minor contributions from fragmented seeds of other Kreutz populations.

7.1. Expanding Spans of Simulated Orbital Elements As a Function of Fragment Generation

The first task I undertook with the simulation code was an investigation of the systematic propagation of perturbations of the seed's orbit, driven by the separation velocities of fragments and manifested by scatter among their orbits. The perturbations were growing with ever increasing number of fragmentation events, described in terms of the number of fragment generations, n_{gen} . For the fragmentation constants, I used — somewhat arbitrarily, but still more or less in line with the arguments in the preceding sections of this paper — the following: $n_{\text{frg}} = 20$, $\Lambda_{\text{min}} = 1$, $\Lambda_{\text{max}} = 2$, $v_{\text{sep}} = 0.2 \text{ m s}^{-1}$, and $t_{\text{ref}} - t_0 = 900 \text{ yr}$.

Because nontidal, cascading fragmentation began near the Sun, continuing toward aphelion, the birth of the *early* fragment generations was confined to relatively small heliocentric distances. As seen from Figure 3, these generations contained a limited number of objects larger than a typical SOHO sungrazer. They have not been included in Figure 5, which begins with the 9th fragment generation and ends with the 16th.

I let the computer code run and sort the sets of the time of return to perihelion, t_π , the longitude of the ascending node, Ω , and the perihelion distance, q . **The difference between the absolutely minimum and maximum values that a pair of simulated fragments of each generation, n , exhibited in each element defined its span, $\text{Sp}_n(t_\pi)$, $\text{Sp}_n(\Omega)$, and $\text{Sp}_n(q)$, respectively.** The number of simulated fragments, equaling 2^n , was increasing from 512 at the 9th generation to 65,536 at the 16th generation. The dimensions of the fragments in this highest generation were 1/40-th part of the seed's dimensions.

Figure 5 confirms that scatter in the orbital elements was growing with increasing fragment generation, as expected. More importantly, the figure also shows that the *rate of increase* in $\text{Sp}_n(t_\pi)$ was diminishing with increasing generation (that is, with time and increasing heliocentric distance), while the parallel rates of increase in $\text{Sp}_n(\Omega)$ and, to a degree, in $\text{Sp}_n(q)$ had a tendency to accelerate. This behavior suggests that scatter in each orbital element was essentially proportional to the magnitude of the perturbation listed in Table 8.

Comparison of the numbers for the 16th generation with the data in Part I is clearly unsatisfactory. The stream's observed duration ever since 1996, now over a period of nearly 30 years, is utterly incompatible with the predicted span of 19 years, from the end of 1996 through early 2016. On the other hand, the range of the longitudes of the ascending node, which for Population I is estimated to cover about 7° , is predicted to extend too wide, over more than 11° , from 358° to more than 9° .

7.2. Spans of Simulated Orbital Elements As a Function of Fragmentation Number, n_{frg}

Throughout the rest of Section 7 the number of fragment generations is being held constant at $n_{\text{gen}} = 16$. In a first step, v_{sep} was kept at 0.2 m s^{-1} and $t_{\text{ref}} - t_0$ at 900 years, while the parameter Λ was varied again between 1 and 2 to plot the dependence of the spans of the three orbital elements on the fragmentation number, n_{frg} , whose allowed range was $17 \leq n_{\text{frg}} \leq 21$. The results are exhibited in Figure 6.

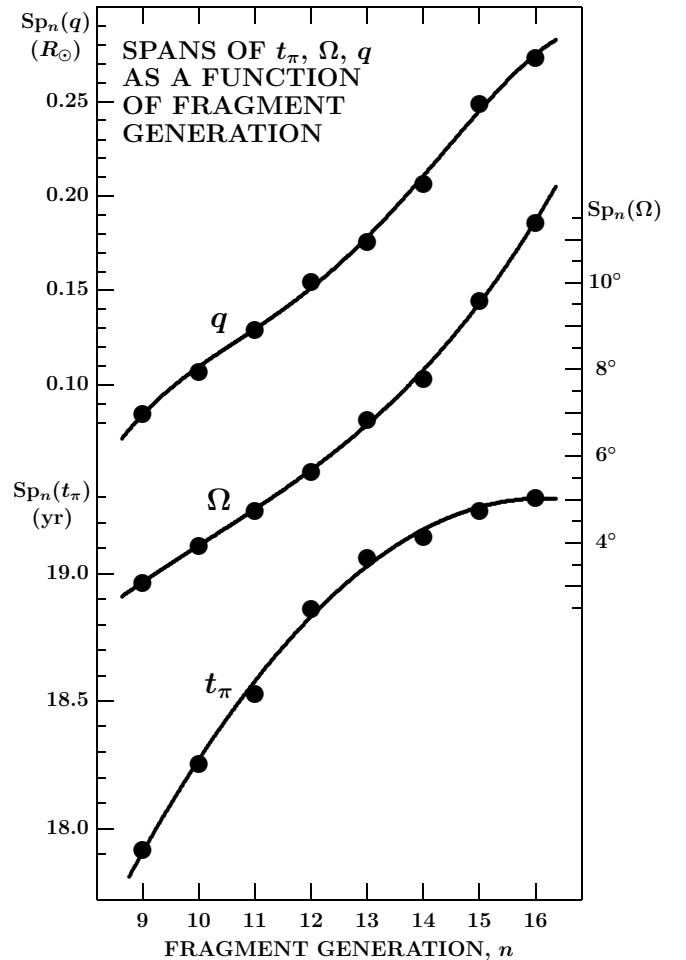


Figure 5. Spans of the times of return to perihelion, t_π , the longitudes of the ascending node, Ω , and the perihelion distances, q , as a function of fragment generation, n , from computer simulation runs based on the following parameters: $n_{\text{frg}} = 20$, $v_{\text{sep}} = 0.2 \text{ m s}^{-1}$, $t_{\text{ref}} - t_0 = 900 \text{ yr}$, $\Lambda_{\text{min}} = 1$, and $\Lambda_{\text{max}} = 2$. Note that the *rate of increase* in $\text{Sp}_n(t_\pi)$ diminishes with time, as the fragmentation process enters ever larger heliocentric distances, while the parallel rates of increase in $\text{Sp}_n(\Omega)$ and, less prominently in $\text{Sp}_n(q)$, continue increasing, in line with the data in Table 8.

The opposite trends between $\text{Sp}_n(t_\pi)$ on the one hand and $\text{Sp}_n(\Omega)$ and $\text{Sp}_n(q)$ on the other hand can be explained by recognizing that an increase in the difference $n_{\text{frg}} - n$ means increasing crowding of the fragmentation times toward smaller heliocentric distance. According to Table 8 the perturbation of t_π increases in that direction, while the perturbations of Ω and q decrease. The spans thus vary qualitatively in line with expectation.

Comparison of the trends in n_{frg} with the observed data from Part I suggests that the smaller the difference between n_{frg} and n , the poorer fit to the data. For the continuing experimentation, it was deemed appropriate to keep n_{frg} at 20.

7.3. Spans of Simulated Orbital Elements As a Function of Parameter Λ

To examine the effect of the parameter Λ on the spans of the orbital elements, I turned off the random number generator for Λ by putting $\Lambda_{\text{min}} = \Lambda_{\text{max}}$. I continued to adopt: $n_{\text{frg}} = 20$, $n = n_{\text{gen}} = 16$, $v_{\text{sep}} = 0.2 \text{ m s}^{-1}$,



Figure 6. Spans of the times of return to perihelion, t_{π} , the longitudes of the ascending node, Ω , and the perihelion distances, q , for simulated fragments of the 16th generation as a function of the fragmentation number, n_{frg} , from computer runs based on the following parameters: $n_{\text{gen}} = 16$, $v_{\text{sep}} = 0.2 \text{ m s}^{-1}$, $t_{\text{ref}} - t_0 = 900 \text{ yr}$, $\Lambda_{\text{min}} = 1$, and $\Lambda_{\text{max}} = 2$. The curve of $\text{Sp}_{16}(t_{\pi})$ now behaves very differently in comparison with those of $\text{Sp}_{16}(\Omega)$ and $\text{Sp}_{16}(q)$, increasing sharply with n_{frg} .

and $t_{\text{ref}} - t_0 = 900 \text{ yr}$. The runs for Λ between 1.1 and 2.3 yielded the results for $\text{Sp}_{16}(t_{\pi})$, $\text{Sp}_{16}(\Omega)$, and $\text{Sp}_{16}(q)$ that are plotted in Figure 7.

It is obvious that Λ affects each of the three spans dramatically, $\text{Sp}_{16}(t_{\pi})$ in particular. However, the variations are now strongly nonlinear, the highest rates being achieved at $\Lambda > 2$ in the time of return to perihelion, but at $\Lambda \rightarrow 1$ in the nodal longitude and perihelion distance. The observed range of 7° in the nodal longitude is matched most closely by $\Lambda \simeq 1.4 - 1.5$, whereas the observed scatter in time nominally requires a minimum $\Lambda \simeq 1.9$. Interestingly, the set for $\Lambda = 1.1$ includes orbits with perihelion distances that are smaller than the Sun's radius.

7.4. Spans of Simulated Orbital Elements As a Function of Separation Velocity

The dependence of the spans of the three elements on the simulated separation velocities of the fragments of the 16th generation is rather straightforward. Computer runs, based on the set of param-

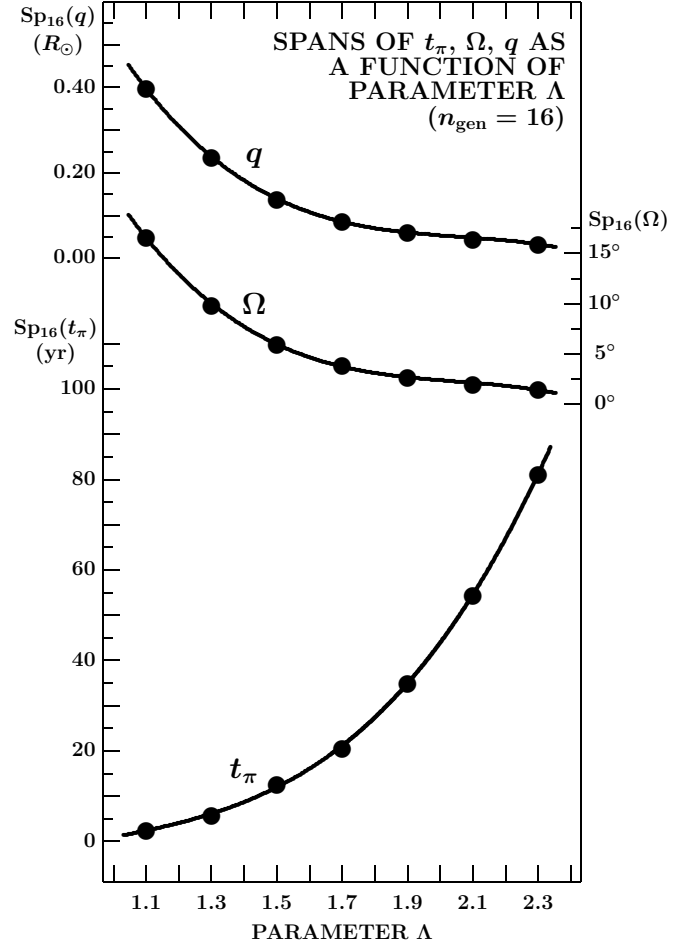


Figure 7. Spans of the times of return to perihelion, t_{π} , the longitudes of the ascending node, Ω , and the perihelion distances, q , for simulated fragments of the 16th generation as a function of the parameter Λ from computer runs based on the following: $n_{\text{frg}} = 20$, $n_{\text{gen}} = 16$, $v_{\text{sep}} = 0.2 \text{ m s}^{-1}$, and $t_{\text{ref}} - t_0 = 900 \text{ yr}$. It is noted that the general trend of the curves is somewhat similar to that in Figure 6 except that the variations are now strongly nonlinear and the spans are much wider.

eters as before ($n_{\text{frg}} = 20$, $n_{\text{gen}} = 16$, $\Lambda_{\text{min}} = 1$, $\Lambda_{\text{max}} = 2$, $t_{\text{ref}} - t_0 = 900 \text{ yr}$), showed that the relationships were nearly perfectly linear, $\text{Sp}_{16}(t_{\pi})$ varying at a rate of 97 yr per 1 m s^{-1} , $\text{Sp}_{16}(\Omega)$ at a rate of 56° per 1 m s^{-1} , and $\text{Sp}_{16}(q)$ at about $1.4 R_{\odot}$ per 1 m s^{-1} . Perihelion distances smaller than $0.7 R_{\odot}$ were obtained in extreme cases. The results, plotted in Figure 8, predict much too high a nodal-longitude rate compared to the rate of arrival times.

7.5. Spans of Simulated Orbital Elements As a Function of Reference Time, t_{ref}

This procedure examines the dependence of the spans of the three elements on the orbital period of the seed, as t_0 is expected to differ at most by a fraction of a day from the perihelion time of the parent comet. The computer runs were based again on the standard parameters: $n_{\text{frg}} = 20$, $n_{\text{gen}} = 16$, $\Lambda_{\text{min}} = 1$, $\Lambda_{\text{max}} = 2$, and $v_{\text{sep}} = 0.2 \text{ m s}^{-1}$. The runs should provide information on the orbital relationship between the seed and the related SOHO sungrazer stream.

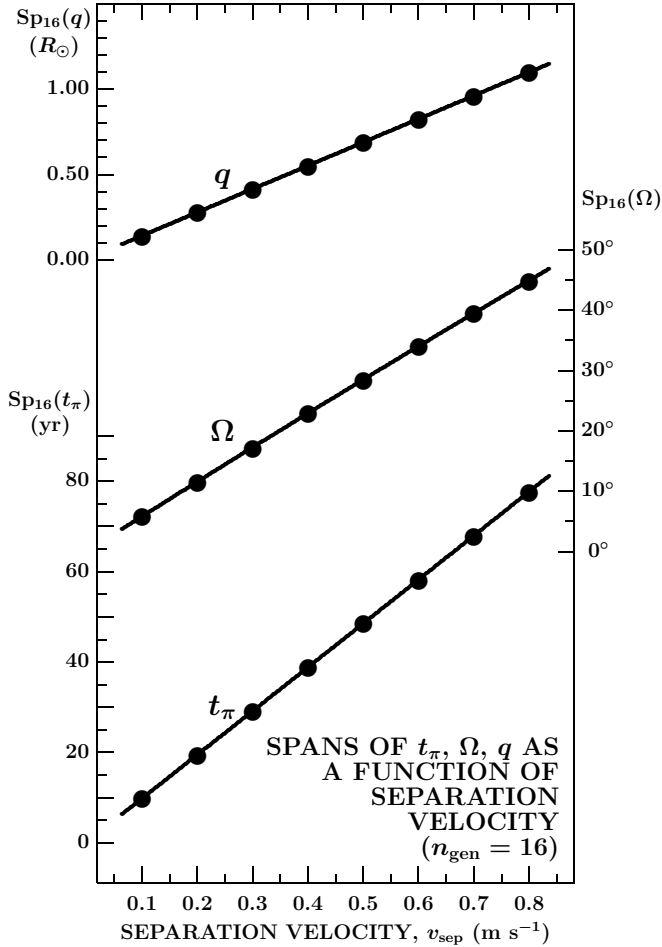


Figure 8. Spans of the times of return to perihelion, t_π , the longitudes of the ascending node, Ω , and the perihelion distances, q , for simulated fragments of the 16th generation as a function of the separation velocity from computer runs based on the following parameters: $n_{\text{frg}} = 20$, $n_{\text{gen}} = 16$, $\Lambda_{\text{min}} = 1$, $\Lambda_{\text{max}} = 2$, and $t_{\text{ref}} - t_0 = 900$ yr. The relationships are nearly perfectly linear.

7.6. Spans of Simulated Orbital Elements As a Function of a Boundary Condition

Usual in problems of this kind is a dependence of results — in this case the spans $\text{Sp}_{16}(t_\pi)$, $\text{Sp}_{16}(\Omega)$, and $\text{Sp}_{16}(q)$ — on boundary conditions. Intuitively, one would expect that the orbital position of the seed at the time of its splitting into the two fragments of the first generation should be instrumental in the process of cascading fragmentation and affect the spans of orbital elements in a profound manner.

Figure 10 shows this expectation to be fully confirmed for the span of the times of return to perihelion, validated to a modest degree for the span of the longitudes of the ascending node, but not corroborated by the span of the perihelion distances, which is independent of the boundary condition. This peculiar outcome of examination of this issue calls for its more extensive investigation.

The nominal results presented in Figures 5 through 9 were based on a few constants (Sections 6.4, 7.1–7.5) and two variables, the parameter Λ and the *vector* of the separation velocity, \mathbf{v}_{sep} , while the *magnitude*, v_{sep} , was kept constant. The variables were controlled by random

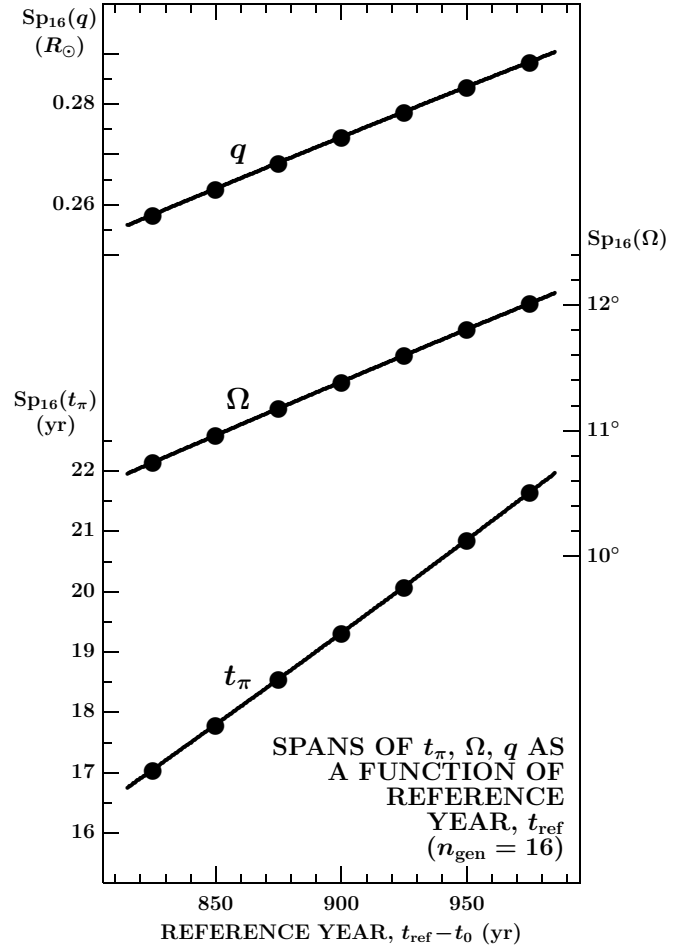


Figure 9. Spans of the times of return to perihelion, t_π , the longitudes of the ascending node, Ω , and the perihelion distances, q , for simulated fragments of the 16th generation as a function of the reference time, t_{ref} , showing an effect of the seed's orbital period. The same parametric values have been used as before: $n_{\text{frg}} = 20$, $n_{\text{gen}} = 16$, $\Lambda_{\text{min}} = 1$, $\Lambda_{\text{max}} = 2$, and $v_{\text{sep}} = 0.2$ m s $^{-1}$.

numbers, the parameter Λ over a wide range. The random numbers $0 < \mathcal{R} < 1$ were read sequentially from a file of one million entries produced by a random-number generator (Section 6.5). The first entry, determining the starting parameter Λ happened to have an extreme value of $\mathcal{R}_0 = 0.9923017714$ (i.e., $\Lambda = 1.9923017714$), implying that the seed split into the first-generation fragments as early as 0.34 day after the parent comet's tidal fragmentation event, at a heliocentric distance of $10.5 R_\odot$. The submeter separation velocities in the opposite directions were enough to get the two fragments into orbits whose periods differed by nearly 11 years: one would have returned to perihelion on 2000 September 29, the other on 2011 August 2. The continuing randomization of the orbital elements of higher-generation fragments led eventually to a span of return to perihelion of nearly 20 years, as shown in the upper left panel of Figure 11 (for $X = 0$). In scenarios in which X was forced to grow, so was the heliocentric distance at the time of the seed's initial breakup, so that the gap between the two peaks in Figure 11, associated with the first-generation fragments, was progressively narrowing down. Accordingly,

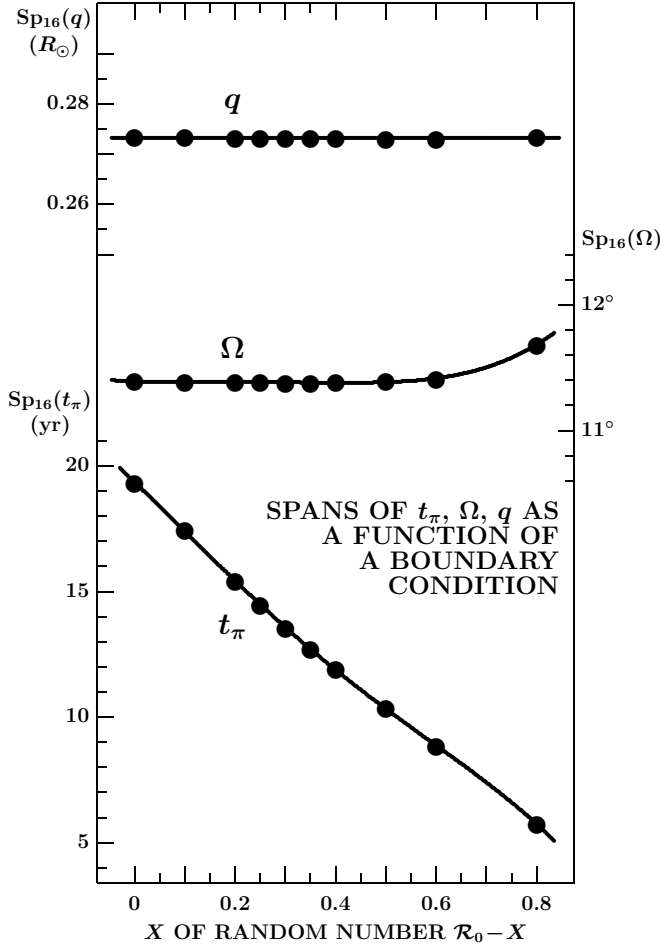


Figure 10. Spans of the times of return to perihelion, t_π , the longitudes of the ascending node, Ω , and the perihelion distances, q , for simulated fragments of the 16th generation as a function of a boundary condition, represented by the first random number $\mathcal{R}_0 = 0.9923017714$ and its forced variations. They controlled the values of Λ and the times of the seed's initial fragmentation. The parameters have remained unchanged: $n_{\text{frg}} = 20$, $n_{\text{gen}} = 16$, $\Lambda_{\text{min}} = 1$, $\Lambda_{\text{max}} = 2$, $v_{\text{sep}} = 0.2 \text{ m s}^{-1}$, and $t_{\text{ref}} - t_0 = 900 \text{ yr}$.

the span of the times of return to perihelion was getting ever shorter. On the other hand, the nodal longitudes of the first-generation fragments essentially coincided, so that the span of the nodal longitudes was unaffected by the increasing values of X until it exceeded ~ 0.5 . For the same reason, the perihelion distances remained independent of the boundary condition for up to X nearing unity ($\mathcal{R} < 0.2$).

7.7. Trends, Constraints, and Conditions

In a way, it was fortunate that the initial random number nearly coincided with the upper boundary, as it led to an unexpected scenario that otherwise may not have been discovered: the first-generation fragments of the seed moved in orbits differing from one another enough to have lasting effect of the orbital evolution of fragments of the 16th generation, causing a two-peaked distribution of their times of return to perihelion (centered on 2001 and 2011/2012). The peaks were separated by a huge gap with no fragments, centered on the projected time of return of the seed (in 2006), as is amply demonstrated by

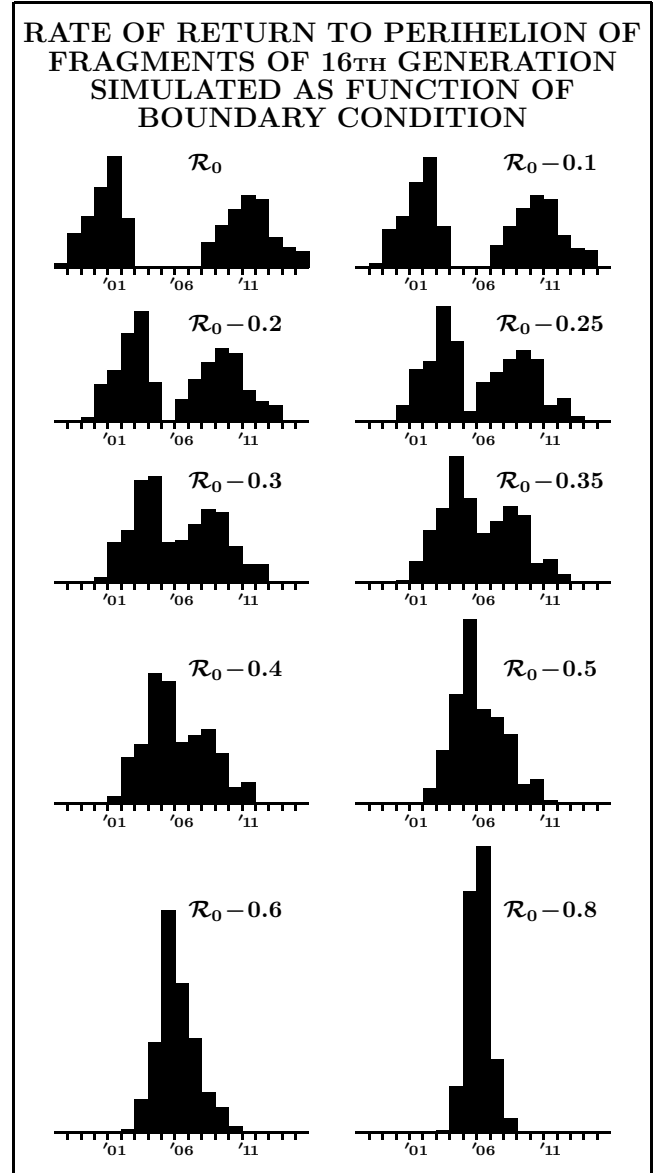


Figure 11. Effects of a boundary condition: Histograms of a rate of return to perihelion of fragments of the 16th generation simulated as a function of the time of the seed's initial breakup into two fragments of the first generation, expressed via the parameter Λ , selected by a random number $\mathcal{R}_0 = 0.9923017714$ and its sequential variations. The times of the seed's initial fragmentation event were, in days following the near-perihelion tidal disruption of the Great Comet of 1106: 0.34 for \mathcal{R}_0 ; 0.85 for $\mathcal{R}_0 - 0.1 = 0.8923 \dots$; 2.2 for $\mathcal{R}_0 - 0.2$; 3.7 for $\mathcal{R}_0 - 0.25$; 6.1 for $\mathcal{R}_0 - 0.3$; 10.3 for $\mathcal{R}_0 - 0.35$; 17.8 for $\mathcal{R}_0 - 0.4$; 54 for $\mathcal{R}_0 - 0.5$; 172 for $\mathcal{R}_0 - 0.6$; and 1933 (or 5.3 yr) for $\mathcal{R}_0 - 0.8 = 0.1923 \dots$. The abscissa shows time in years ('01 stands for 2001, etc.); the ordinate, uniform throughout, displays the annual rate of return to perihelion of simulated 16th generation fragments; for example, the highest rate at the upper left panel is 11,041 fragments per year (in 2001), the highest rate at the bottom right panel is 28,364 fragments per year (in 2006). It is noted that, especially in the upper four histograms, the distributions are prominently double-peaked because the seed split into two first-generation fragments of very different orbital periods, one returning to perihelion in September 2000, the other in August 2011, at times that the peaks are centered on. The projected return of the seed, in early 2006, approximately coincides with the center of the wide gap. On the other hand, the distributions in the last three histograms are increasingly sharp-peaked on the year of 2006, as at these values of Λ the projected perihelion returns of the first generation fragments and their successive products nearly coincided with the projected return of the seed.

the panels in the two upper rows of Figure 11. However, when I forced the initial random number \mathcal{R}_0 to attain progressively lower values, the two peaks gradually became less prominent, the gap between them shrinking and getting more shallow. At $\mathcal{R}_0=0.4$ one peak was on the verge of disappearance, the span of the times of return to perihelion continuing to diminish. Eventually, the single peak near the seed’s projected time of return to perihelion became prominent and narrow as \mathcal{R}_0 continued to decrease toward its lower boundary of zero. This was a shape of the distribution of perihelion arrival times that better met one’s expectation.

The peak arrival rates that I was getting are seen from Figure 11 to reach about 10^4 SOHO-like sungrazers per year (sic!), or *two orders of magnitude* too high in comparison with the observations that were mentioned in Part I [and here is Section 6.1 and Equation (62)]. Furthermore, to be in line with the data, the span of the times of return to perihelion in Figure 10 should be wider by a factor of at least 2 to 5 (for the stream to last an absolute minimum of 30 years). On the other hand, the span of the longitudes of the ascending node should be narrower to better fit the width of 7° , estimated for Population I in Part I. It is obvious that while the exercises performed in Sections 7.1 through 7.6 were useful in terms of learning the effects of the various parameters on the spans of the three orbital elements, the values used were apparently nowhere near those needed to fit the observed stream of SOHO sungrazers.

7.7.1. Attempting Corrective Actions

For a given n_{gen} and a number of objects, the annual arrival rate must drop when a span of the times of return to perihelion broadens. This was one of the rules followed in an effort to rectify the problems with the high rates. To find appropriate values of the parameters, I focused on two key issues: (i) to fit the slope and end points of the arrival rate of Population I sungrazers observed in the C2 coronagraph in the years 2000–2009 — I opted for the rates corrected for the missed data, 120 objects in 2000 and 200 objects in 2009 (Section 6.1); and (ii) to match the range of the corrected longitudes of the ascending node of these objects. Also taken into account were other well-known properties of the stream of SOHO sungrazers, such as (iii) an essentially constant rate of arrivals after 2009 (Battams & Knight 2017),⁷ a conclusion believed to be in general valid for Population I as well, even though its membership was less clear in the absence of orbital information after 2010; and (iv) evidence of post-aphelion fragmentation events from detection of close pairs of sungrazers (Sekanina 2000).

Given the degree of stochasticity, the search for the “best” solution had to be conducted by trial and error, with hardly any interpolation possible. The constraints provided by the simulated distribution of the longitudes of the ascending node proved decisive, as they ruled out separation velocities higher than 0.7 m s^{-1} , which would have led to an unacceptably wide range of these nodal longitudes.

⁷ An anomaly was the arrival of a swarm of bright Population I sungrazers, detected in the years 2009 through 2012. The peak rates were 4.6 per year in late 2010 for the objects brighter at maximum light than magnitude 3 and 4.3 per year in early 2011 for the objects brighter than magnitude 2 (Sekanina & Kracht 2013).

The limits dictated by the nodal-longitude conditions did unfortunately have a very detrimental effect on the options left open to modeling the annual arrival rates of the stream sungrazers. The extremely high rates would have been brought down at least to a degree by higher separation velocities, because they would have stretched arrivals over wider periods of time. With this option now unavailable, the only way left to bring the arrival rates in 2000–2009 down to 120–200 objects per year was to accept that these years were near the beginning of the span of the times of return to perihelion.

The best bet was to elevate Λ to values near 2 to curtail the number of fragmentation events at larger heliocentric distances, where the nodal longitudes get perturbed more strongly, and to move the seed’s projected arrival time far into the future by choosing a proper value of $t_{\text{ref}}-t_0$. In spite of the two caveats regarding $\Lambda > 2$ [one in Section 4 and Equation (41), the other in Section 6.3 and Table 11], neither objection ruled out maximum values of Λ near 2.1, so long as Λ remained a random variable with a lower limit below 2.

7.7.2. Rejection of SOHO Sungrazer Stream Models Based on 16 Fragment Generations

These efforts notwithstanding, it was not possible to avoid a continuing rise of the simulated arrival rates at times following the tested period of 2000–2009. The rates reached absurdly high levels, exceeding 900 objects per year (sic!) at maximum in the mid-21st century and they topped 350 objects per year in the early 2020s, which we now know for sure to be much too high.

An example of the arrival rate of the stream of SOHO sungrazers of Population I, simulated as consisting of 65,500 16th generation fragments of a seed born at near-perihelion tidal breakup of the parent comet X/1106 C1, is displayed in Figure 12. The fragments stretched over about 190 years, thus averaging about 350 objects per year. I came up with a number of alternative scenarios, all of which rather closely resembled the plotted one. To bring the rate down to less than 200 objects to get it in line with the observations would have required that the stream stretched over more than four centuries, an unacceptable condition.

The treatment of the SOHO sungrazers as fragments of the 16th generation was based on a probable seed-to-sungrazer size ratio of about 40 — a seed of 400 meters in diameter and a SOHO sungrazer 10 meters across. This ratio, which up to this point was the most fundamental constant of these computations, could not be sustained dynamically, leading for Population I to a stream about four times as dense as is the observed stream. Accordingly, in the framework of the methodology employed in this investigation, *all sungrazer stream models based on the premise that the SOHO sungrazers are fragments of the 16th generation must be rejected*. The degree of disparity suggests that the seed-to-sungrazer size ratio has to be reduced by a factor of about $4^{\frac{1}{3}} \simeq 1.6$, from 40 down to 25; the SOHO sungrazers of Population I should be treated as *fragments of the 14th generation*, whose total number from a single seed is $2^{14} \simeq 16,400$. Considering that, *after corrections*, the number of “known” members of this population should amount to more than 4000, at least a quarter of the stream is already on the books, not including the part before 1996.

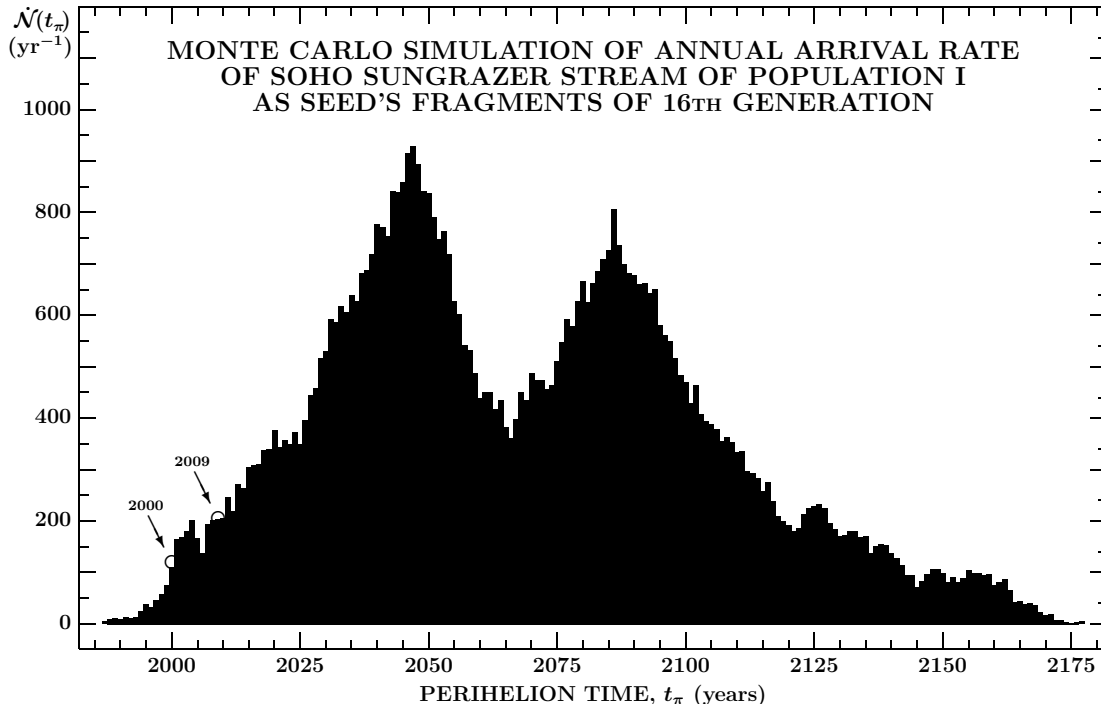


Figure 12. Simulation of an arrival rate \dot{N} (per year) of the stream of SOHO sungrazers of Population I as fragments of the 16th generation of a seed born at near-perihelion tidal breakup of comet X/1106 C1. Other parameters of the simulation curve: $n_{\text{frg}} = 20$, $\Lambda_{\text{min}} = 1.93$, $\Lambda_{\text{max}} = 2.13$, $v_{\text{sep}} = 0.69 \text{ m s}^{-1}$, $t_{\text{ref}} - t_0 = 962 \text{ yr}$. The two peaks measure the difference between the orbital periods of the two fragments of the first generation. The shapes of these simulation curves are largely independent of the boundary condition. The simulated arrival rates, $\dot{N}(2000) = 110 \text{ yr}^{-1}$ and $\dot{N}(2009) = 203 \text{ yr}^{-1}$, are compared with the corrected rates derived from the data, 120 and 200 yr^{-1} , respectively, depicted by open circles. The arrival-rate curve is grossly inconsistent with the observed arrival rates outside the interval 2000–2009, implying 350 arrivals per year in the early 2020s; all models simulating the stream of SOHO sungrazers as fragments of the 16th generation failed miserably.

One should add two caveats. Contemplating the reduction of the size ratio between the seed and a SOHO-like sungrazer, one should remember that all fragments of a given generation are assumed to be of equal size. Accordingly, by the size of a SOHO sungrazer one should understand the dimensions of an *average* member of this category, not of the most common (smallest detected) member. It very well may be this difference that takes care of the discrepancy; one only needs to replace the diameter of 10 meters with 16 meters, a difference too subtle to argue about.

The other caveat concerns the seeds. There is no doubt that a single tidal breakup of the parent comet generates a number — probably a large number — of seeds, whose orbital periods differ to various degrees. If the SOHO-like sungrazer debris from a single seed gets scattered over an arc of the orbits equivalent to a span of two centuries, the debris from any two seeds may or may not overlap, scenarios that could further complicate the interpretation of the sungrazer stream data.

8. RESULTS FOR FRAGMENTS OF 14TH GENERATION: A SUCCESS

Already the earliest computer runs for $n_{\text{gen}} = 14$ suggested that the problems with high arrival rates were gone. The trial and error approach led to major differences in some parameters in comparison with runs for $n_{\text{gen}} = 16$. Probably the most significant was the shift in $t_{\text{ref}} - t_0$. While runs for the 16th fragment generation predicted values near 960 years, indicating that its

original orbit would bring the seed back to perihelion in the late 2060s, runs for the 14th generation led to times about 30 years earlier. This shift moved the main peak in Figure 12 from the late 2040s by just about the same amount of time, while the secondary peak in Figure 12 now disappeared.

An example of the arrival-rate simulation curve for the stream of SOHO sungrazers of Population I, established from an excellent Monte Carlo run based on fragments of the 14th generation, is displayed in Figure 13 and its parameters are listed in Table 13. The plot offers several predictions: (i) the stream should survive for almost exactly 200 years, from about 1950 to 2150, even though over the last 50 years the arrival rate is expected to average less than 1 sungrazer per week and in the last decade or so less than 1 sungrazer per month; (ii) the stream should have peaked in the 2010s, when the arrival rate of the sungrazers detected in the C2 coronagraph (and corrected for the missed ones) should have attained about 220 per year; the peak appears to be a product of fragmentation of one of the two parts of the seed that ended up in an orbit that would have brought it back to perihelion in June 2011; (iii) perhaps significantly, the timing of the peak essentially coincides with the reported arrival of a swarm of bright SOHO sungrazers (Sekanina & Kracht 2013), of magnitude not fainter than 3 at maximum light; these could be larger fragments of the same part of the seed, whose fragmentation had stopped or was slow; and (iv) values of the parameters of the simulated arrival-rate curve were searched for by trial and error to approxi-

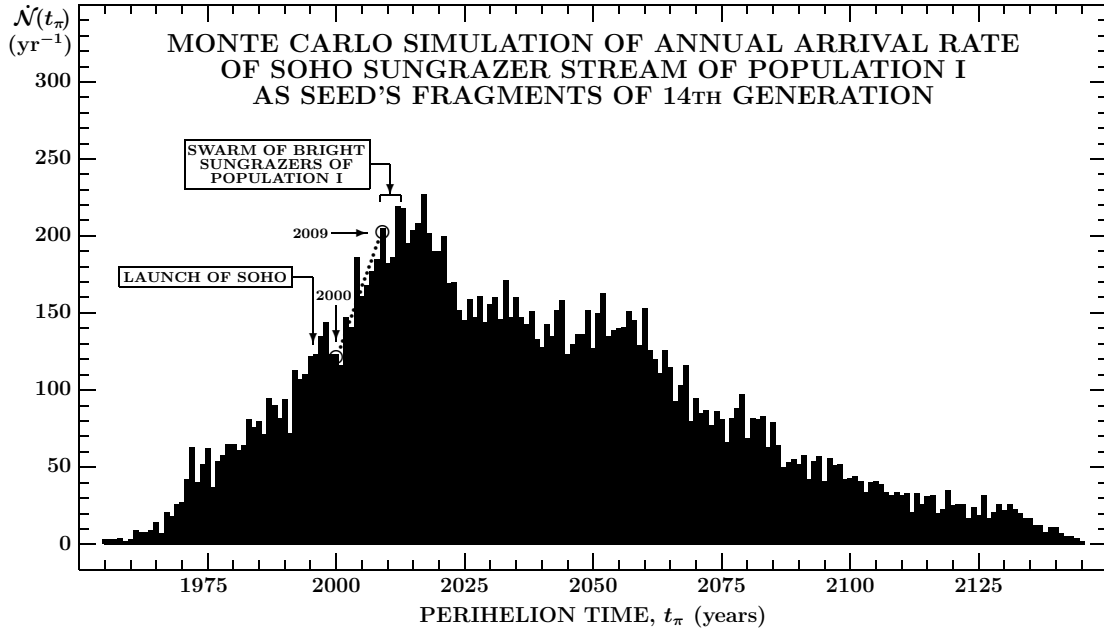


Figure 13. Successful simulation of an arrival rate \dot{N} (per year) of the stream of SOHO sungrazers of Population I as fragments of the 14th generation of a seed born at near-perihelion tidal breakup of comet X/1106 C1. Other parameters of the simulation curve: $n_{\text{frg}} = 20$, $\Lambda_{\text{min}} = 1.6$, $\Lambda_{\text{max}} = 2.1$, $v_{\text{sep}} = 1.20 \text{ m s}^{-1}$, $t_{\text{ref}} - t_0 = 930 \text{ yr}$. The peak measures the orbital period of one of the two fragments of the first generation, which would have passed perihelion in June 2011. The shapes of these simulation curves are largely independent of the boundary condition. The simulated arrival rates, $\dot{N}(2000) = 123 \text{ yr}^{-1}$ and $\dot{N}(2009) = 205 \text{ yr}^{-1}$, are compared with the corrected rates derived from the data, 120 and 200 yr^{-1} , respectively, depicted by the open circles. Also shown are the launch of the SOHO observatory and the detection of a swarm of bright SOHO sungrazers (of peak magnitude not fainter than 3) in 2009–2012 (Sekanina & Kracht 2013), a coincidence that may corroborate the predicted time of the stream’s maximum arrival rate.

mately fit the corrected rates of $\dot{N}(2000) = 120$ per year and $\dot{N}(2009) = 200$ per year, as established for Population I in Part I; this was the only constraint used from the stream’s arrival rates.

The separation velocity in Table 13 is surprisingly high compared to the range of values contemplated in Section 3.3 and Table 6. The disparity has two important implications. One is an effect on the relationship between the separation velocity and what I took to be a *tensile* strength of the fragments. In retrospect, the involved quantity of σ_{T} should better be called a *cohesion* strength, for which v_{sep} from Table 13 implies a value of about 2700 Pa, more than one order of magnitude higher than the tensile strength of comets is believed to average. The second implication concerns the rotation period of the minor sungrazers, which appears to be on the order of 1 minute if not shorter.

Another constraint was provided by the span of nodal longitudes. For the period from 1996 through mid-2010

the distribution of 390 members of Population I from the corrected Marsden data was plotted in Figure 3 of Part I, showing the nodal longitudes in a range of about 7° , from 359.5 to 6.5 . The sungrazer stream simulated here by fragments of the 14th generation offers a very good match; for the period from 1996 through mid-2010 the histogram is plotted in Figure 14, for the 2000–2009 period in Figure 15. Both plots show a clear peak at the longitude of the ascending node of the parent comet (and the parent seed), as expected. The range of the longitudes is slightly shifted to higher values, but the contamination by the excess beyond 6.5 is less than 2 percent. The three potential swarms are not seen in the simulation, but this is not surprising given that the observations provided only an average of about 11 data points per 0.2 wide interval of longitude, thus failing to prevent significant scatter.

For the sake of interest, I also provide, in Figure 16, a histogram of the distribution of perihelion distances among simulated fragments of the 14th generation in the 2000–2009 period. As already noted in Part I, unlike the longitude of the ascending node, the perihelion distance of the Marsden gravitational orbits for the SOHO sungrazers cannot be corrected for effects of the nongravitational acceleration and, as a result, can provide no additional orbital information on the fragmentation process. This point is supported by Figure 16, which predicts the simulated distribution of fragments’ perihelion distances to be confined to between 1.08 and $1.28 R_{\odot}$, while the orbital data show about 10 percent of the Population I sungrazers from the 2000–2009 period to have perihelia beyond $1.5 R_{\odot}$.

Table 13

Parameters of the Monte Carlo Model
for the Stream of SOHO Sungrazers of Kreutz Population I
As Fragments of a Seed (Parent Comet X/1106 C1)

Parameter	Value
Fragment generation, n_{gen}	14
Fragmentation number, n_{frg}	20
Range of slowdown parameter, Λ	1.6–2.1
Separation velocity, v_{sep}	1.2 m s^{-1}
Reference time, $t_{\text{ref}} - t_0$	930 yr

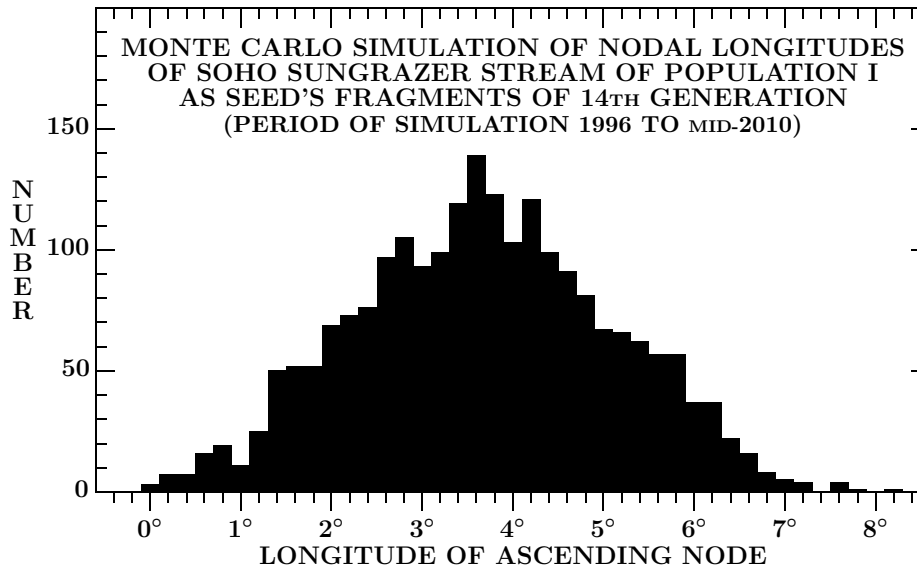


Figure 14. Histogram of the Monte Carlo simulated longitudes of the ascending node for the stream of SOHO sungrazers of Population I, modeled as 14th generation fragments of a seed. The selected period is 1996 to mid-2010, the time interval for which Marsden’s gravitational orbits were available. Note a good match to the observed range of nodal longitudes of 7°, from 359°.5 to 6°.5, presented in Part I.

9. SUMMARY AND CONCLUSIONS

This Part II completes the first serious effort aimed at providing a physical model for the stream of SOHO sungrazers⁸ of the Kreutz system. Even though the first SOHO sungrazers, which have for nearly 30 years been dominated by the Kreutz comets, were not detected until more than two years after the space observatory’s launch, the pace has been accelerating over the years thanks to spontaneous enthusiasm of participating amateur comet hunters, and a celebration of the discovery of the incredible 5000th object is still in progress as these lines are being written!

The stream of Kreutz sungrazers is complex because the Kreutz system is complex, consisting of a number of populations of genetic significance. This investigation deals with the stream of only one of them — Population I, which was introduced by Marsden (1967) as Subgroup I and which has ever since 1996 been the main contributor to the SOHO sungrazer stream. One can take a view that the observed stream consists of a number of individual streams, each population having its own. Whether or to what extent is a model for one stream useful to formulating models for the others remains to be determined.

While the sections of this paper have been organized thematically, the summary is arranged chronologically, which the reader may prefer. One point concerning the stream of SOHO sungrazers that is unlikely to invite any controversy is a declaration that the stream consists of fragments of a larger, parent body or bodies. Speaking of the Kreutz system as a whole, the ultimate par-

ent was the progenitor, which my recent contact-binary model (Sekanina 2021b) identifies with Aristotle’s comet of 372 BC. Speaking more specifically of Population I, as I do in this investigation, a more direct parent was this population’s principal mass, which in my model was the Great Comet of 1106 (X/1106 C1). But I propose that the *immediate* parent of the sungrazer stream that the SOHO’s coronagraphs see was a subkilometer-sized fragment of the 1106 comet, which separated from it (with many other objects of different sizes, both larger and smaller) in the course of an event of tidal fragmentation in close proximity of perihelion, at the beginning of February 1106. I refer to this immediate parent as a *seed*. I believe that the seed of the SOHO sungrazer stream of Population I was a single object, even though it is virtually certain that there were many seeds, each generating its own stream at some time. Streams of different seeds may, but do not have to, overlap one another. From the limited data available I have as yet seen no evidence that would contradict the premise of a single seed.

Not every fragment of the parent comet can become a seed. A seed has to be resilient and large enough to survive on its own the first hours after birth in the harsh environment of the solar corona, yet in the long run it should be brittle enough to be prone to progressive fragmentation. Objects like comet Lovejoy (C/2011 W3), which was not a member of Population I, or the Great Southern Comet of 1887 (C/1887 B1), which was, may be appropriate seed prototypes. Their existence suggests that the formation of a SOHO-like stream does not have to be necessarily linked to the perihelion passage of a major Kreutz sungrazer, even though in most cases it probably is.

Modeling of a seed’s fragmentation process leading to a SOHO-like stream consists of handling two different issues: (i) repetitive scaling down of a rotationally-induced fragmentation event whose product is assumed to be self-similar and (ii) a distribution law for the sequence of such

⁸ I keep referring to the *SOHO sungrazer stream*, but the imagers on board the *STEREO* spacecraft (and, very recently, the *Parker Solar Probe*) should also be acknowledged for contributing to the stream’s observation. And to the extent that one could speak of streams made up of fewer than two dozen comets, the same applies to the imagers on board the *Solwind* (P78-1) and *Solar Maximum Mission* satellites in 1979–1989. My reference to the SOHO stream is merely a short-cut term that recognizes SOHO’s data and dominant position in this field of scientific activity.

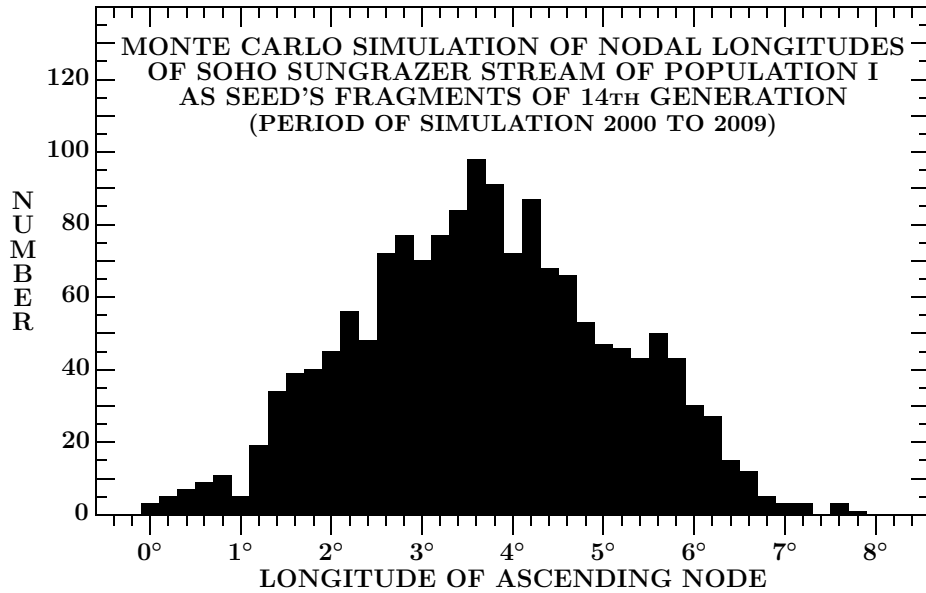


Figure 15. Histogram of the Monte Carlo simulated longitudes of the ascending node for the stream of SOHO sungrazers of Population I, modeled as 14th generation fragments of a seed. The selected period is 2000 to 2009, used in Figure 13 to fit the arrival-rate curve. Note a good match to the observed range of nodal longitudes of 7° , from 359.5 to $6^\circ.5$, presented in Part I.

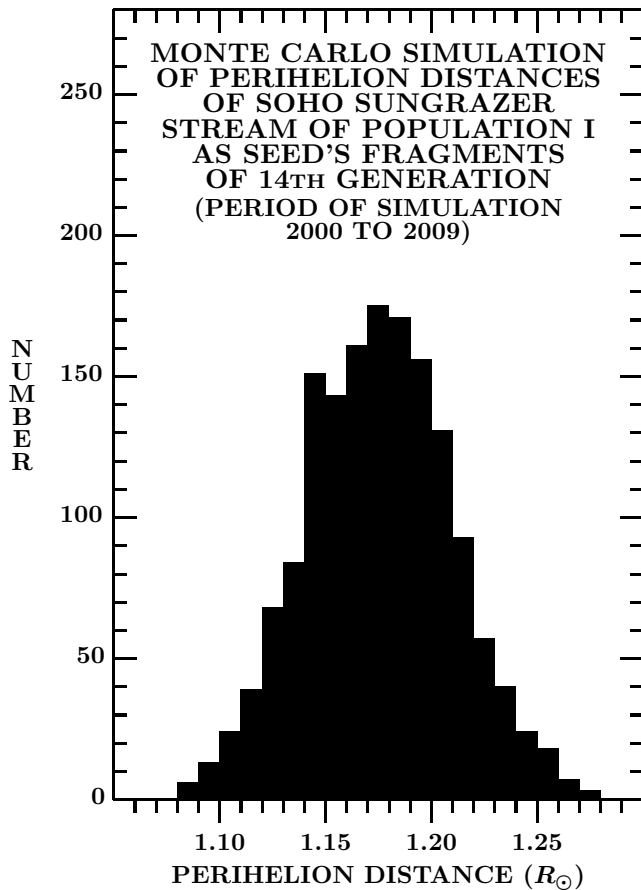


Figure 16. Histogram of the Monte Carlo simulated perihelion distances for the stream of SOHO sungrazers of Population I, modeled as 14th generation fragments if a seed. The selected period is 2000 to 2009, used in Figure 13 to fit the arrival-rate curve. Unfortunately, this distribution cannot be tested on a set of observed perihelion distances, because the available data are not even approximately corrected for major nongravitational effects.

fragmentation events along the orbit. Since all fragments are irregular in shape, their figure is ignored when developing the algorithm for solving the first problem. At the same time, the fragment size is linked to the number of events by postulating that, in each fragmentation episode, a spherical object breaks into two equal halves. This procedure is easy to handle mathematically, introducing a dependence on the material's tensile or, rather, cohesive strength against rotational fragmentation. The value of this quantity is determined indirectly, via a separation velocity. Its *magnitude* is assumed to be constant, which implies a spinup as the fragments' dimensions diminish with time. On the other hand, as the fragments are expected to tumble uncontrolably, the separation velocity *vector* is allowed to vary at random. In practice, its RTN components are determined by a random-number generator.

The separation velocity vector serves as a perturber of fragments' paths, which is ultimately responsible for orbital scatter of the sungrazer stream. The section on the perturbations demonstrates in some detail, how the contributions to the radial, transverse, and normal components of the separation velocity project as variations in the orbital period, the perihelion distance, and the longitude of the ascending node. The orbital position at the time of fragmentation plays an important role in determining the amounts of change in the various orbital elements.

These effects are in the paper described by a law, whose beginnings date to my early investigation of cascading fragmentation (Sekanina 2002) to replace the traditional view that sungrazers split only at perihelion. Based in part on Sekanina et al.'s (1998) experience with a breakup sequence of the ill-fated comet Shoemaker-Levy (D/1993 F2), evidence suggested that the fragmentation rate was tapering off — the reason for introducing the “slowdown” parameter Λ (Sekanina 2002).

Among the additional parameters of the proposed geometric progression of fragmentation times, the most important is the number of fragment generations, n_{gen} . Because any fragment is considered to split into two equal subfragments, there is a relationship between the number of fragments and the number of their generations. This rule also resolves the issue of the fragments' momentum exchange at breakup. Potentially confusing is the meaning of the fragmentation number, n_{frg} . As introduced in Section 4, all fragments of the n_{frg} -th generation return to perihelion at the same time, regardless of Λ , as shown in Table 7. But sungrazers of course return to perihelion at very different times, when $n < n_{\text{frg}}$. The fragmentation law is incorporated into the Monte Carlo simulation routine in Section 6.3, in which the number of fragment generations, n_{gen} , needed to fit the observed arrival rate of SOHO sungrazers, is introduced. The arrival rate also depends on the seed's initial orbital period.

The stochastic nature of the fragmentation process is assumed to be determined primarily by the complex sequence of fragmentation events, their timing on the one hand, and by chaotic rotation of fragments, which results in their unpredictable momentum changes at each event, on the other hand. These circumstances have dictated the need for application of a Monte Carlo simulation approach.

Certain aspects of the fragmentation problem are, for better or worse, treated deterministically. For example, all SOHO sungrazers are treated as fragments of the same generation and equal dimensions. Similarly, I assume a constant size (and mass) ratio between the seed and a fragment. As already noted, the magnitude of separation velocities is also kept constant. The values of the slowdown parameter Λ are subject to random variations, but only within a prescribed range.

In conclusion, one of the prime objectives — to fit the annual arrival rate of the SOHO sungrazers of Population I over a period of 10 years — has been achieved in Figure 13. The rates, from 120 per year in 2000 to 200 per year in 2009, have rested on the counts in the C2 coronagraph, corrected for missed objects due to seasonal effects. A search by trial and error suggests that a successful solution requires that the SOHO sungrazers be 14th generation fragments, which implies a total number of 2^{14} or about 16,400 objects and a 25:1 size ratio between the seed and an average sungrazer; for example, a seed 400 meters in diameter requires that an average sungrazer be 16 meters across. The second prime objective — to fit the observed range of 7° in the longitude of the ascending node of the sungrazers, from 359.5 to 6.5 — has been taken care of in Figures 14 and 15.

The stream's activity is predicted to last for 200 years, from about 1950 to about 2150, suggesting that by the end of 2023 approximately 42 percent of the stream's sungrazers had already arrived. The stream is predicted to have culminated in the 2010s. Interestingly, a swarm of bright SOHO sungrazers of Population I (not fainter than magnitude 3 at peak light) appeared in 2009–2012 (Sekanina & Kracht 2013). These could be fragments of the seed that either ceased breaking up early or have been fracturing at much slower rates. On its initial orbit, whose period was 193 years longer than the orbital period of X/1106 C1's principal fragment, C/1843 D1, the seed would arrive in 2036.

My description on the proposed Monte Carlo model for the SOHO sungrazer Population I stream comes here to an end. Although not directly related to the topic, I still should point out that computations carried out in Section 2.3 suggest that the apparent tidal disruption of the parent comet X/1106 C1, which appears to have triggered the birth of the stream, may also account for C/1668 E1 and a possible major fragment that could arrive in the 2050s or 2060s.

It is my sincere hope that this paper will offer a good starting position for more ambitious investigations in the future.

REFERENCES

- Attree, N., Groussin, O., Jorda, L., et al. 2018, *A&A*, 611, A33
 Battams, K., & Knight, M. M. 2017, *Phil. Trans. Roy. Soc. A*, 375, 20160257
 Boehnhardt, H. 2002, *Earth Moon Plan.*, 89, 91
 Davidsson, B. J. R. 2001, *Icarus*, 149, 375
 Delsemme, A. H., & Miller, D. C. 1971, *Plan. Space Sci.*, 19, 1229
 Gould, B. A. 1891, *Result. Obs. Nacion. Arg.*, 13, 600
 Green, D. W. E. 2011, *IAU Circ.* 9246
 Groussin, O., Jorda, L., Auger, A., et al. 2015, *A&A*, 583, A32
 Hamid, S. E., & Whipple, F. L. 1953, *AJ*, 58, 100
 Henderson, T. 1843, *Astron. Nachr.*, 20, 333
 Hufnagel, L. 1919, *Astron. Nachr.*, 209, 17
 Jewitt, D. 1997, *Earth Moon Plan.*, 79, 35
 Jewitt, D. 2021, *AJ*, 161, 261
 Jewitt, D. 2022, *AJ*, 164, 158
 Knight, M. M., A'Hearn, M. F., Biesecker, D. A., et al. 2010, *AJ*, 139, 926
 Kreutz, H. 1891, *Publ. Kiel Sternw.*, 6
 Kreutz, H. 1901, *Astron. Abhandl.*, 1, 1
 MacQueen, R. M., & St. Cyr, O. C. 1991, *Icarus*, 90, 96
 Marsden, B. G. 1967, *AJ*, 72, 1170
 Marsden, B. G. 1989, *AJ*, 98, 2306
 McCauley, P., Saar, S. H., Raymond, J. C., et al. 2013, *ApJ*, 768, 161
 Michels, D. J., Sheeley, N. R., Jr., Howard, R. A., & Koomen, M. J. 1982, *Science*, 215, 1097
 Raymond, J. C., Downs, C., Knight, M. M., et al. 2018, *ApJ*, 858, 19
 Seargent, D. 2009, *The Greatest Comets in History: Broom Stars and Celestial Scimitars*. New York: Springer Science+Business Media, LLC, 260pp
 Sekanina, Z. 1982, in *Comets*, ed. L. L. Wilkening (Tucson: Univ. Arizona), 251
 Sekanina, Z. 1984, *Icarus*, 58, 81
 Sekanina, Z. 2000, *ApJ*, 542, L147
 Sekanina, Z. 2002, *ApJ*, 566, 577
 Sekanina, Z. 2003, *ApJ*, 597, 1237
 Sekanina, Z. 2021a, eprint arXiv:2110.10889
 Sekanina, Z. 2021b, eprint arXiv:2109.01297
 Sekanina, Z. 2022a, eprint arXiv:2212.11919
 Sekanina, Z. 2022b, eprint arXiv:2211.03271
 Sekanina, Z., & Chodas, P. W. 2007, *ApJ*, 663, 657
 Sekanina, Z., & Chodas, P. W. 2008, *ApJ*, 687, 1415
 Sekanina, Z., & Chodas, P. W. 2012, *ApJ*, 757, 127
 Sekanina, Z., & Kracht, R. 2013, *ApJ*, 778, 24
 Sekanina, Z., & Kracht, R. 2015a, *ApJ*, 815, 52
 Sekanina, Z., & Kracht, R. 2015b, *ApJ*, 801, 135
 Sekanina, Z., & Kracht, R. 2022, eprint arXiv:2206.10827
 Sekanina, Z., Chodas, P. W., & Yeomans, D. K. 1998, *Plan. Space Sci.*, 46, 21
 Sheeley, N. R., Jr., Howard, R. A., Koomen, M. J., & Michels, D. J. 1982, *Nature*, 300, 239
 Strom, R. 2002, *A&A*, 387, L17
 Vincent, J.-B., Hviid, S. F., Mottola, S., et al. 2017, *Mon. Not. Roy. Astron. Soc.*, 469, S329
 Warner, B. 1980, *Mon. Not. Astron. Soc. South Africa*, 39, 69
 Whipple, F. L., & Stefanik, R. P. 1966, *Mém. Soc. Roy. Sci. Liège* (Sér. 5), 12, 33
 Ye, Q., Jewitt, D., Hui, M.-T., et al. 2021, *AJ*, 162, 70